Experimental analysis of aging

S. Ciliberto
Ecole Normale Supérieure de Lyon, Laboratoire de Physique ,
C.N.R.S. UMR5672,
46, Allée d'Italie, 69364 Lyon Cedex 07, France

August 11, 2003

Abstract

Several experimental aspects of the aging dynamics are discussed. We first introduce the general features of aging. We then describe several experimental procedures, based on the response function, which have been useful to study memory and rejuvenation effects in various materials. A comparison of the results obtained in the different materials is done. The experimental analysis of the violation of the fluctuation-dissipation theorem (FDT) in aging materials is presented. We describe several experiments where the violation has been studied in some details. The amplitude, the persistence time and the observable dependence of the violation observed in the experiments are analyzed. The relevance of these experimental results for recent models of aging is discussed.

1 Introduction

Many physical systems in nature are not in thermodynamic equilibrium because they present very slow relaxation processes. A typical example of this phenomenon is the aging of glassy materials: when they are quenched from above their glass transition temperature T_g to a temperature $T < T_g$, any response function of these systems depends on the aging time t_w spent at T. For example, the dielectric and elastic constants of polymers continue to evolve several years after the quench [1]. The magnetic susceptibility of spin-glasses depends on the time spent at low temperature [2]. Another example of aging is given by colloidal-glasses, whose properties evolve during the sol-gel transition which may last a few days [3]. An important feature of aging materials is the dependence of their physical properties on the thermal history of the sample. Indeed experimental procedures, based on multiple cycles of cooling, heating and waiting times, have shown the existence of two spectacular effects: memory and rejuvenation. Specifically, aging materials present a rejuvenation for any negative temperature perturbation and at the same time during heating they remind the stops at fixed temperature done during cooling (see for example [4, 5] and references therein). In the first part of this lecture we will describe these two effects and the experimental procedures used to characterize them. These procedures have been extremely useful to fix

several constraints for the phenomenological models [6, 7] and thus they merit to be described in some details.

In the second part of the lecture we will address another important problem of the aging dynamics. Indeed glasses are out of equilibrium systems and usual thermodynamics does not necessarily apply. However, as the time evolution is slow, some concepts of the classical approach may be useful for understanding the glass aging properties. A widely studied question, is how the temperature of these systems can be defined. One possible answer comes from the study of the deviation to the Fluctuation Dissipation Theorem (FDT) in an out of equilibrium system (for a review see ref.[9, 10] and Cugliandolo lecture in these proceedings). In this lecture we will describe a series of experiments where this question is analyzed in some details on real materials. The implications of these experimental results on the models of aging are finally discussed.

2 Aging, memory and rejuvenation

The aging of glassy materials is a widely studied phenomenon [1, 2] which is experimentally analyzed by measuring as a function of time the dielectric susceptibility, the elastic constants, the density and the thermal properties of the materials. In the next subsection we will give an example of the aging of the dielectric constant of plexiglass (PMMA), which is a polymer glass with $T_g = 388K$ [12]. We will show first the aging properties and then, in the next sections the memory effects in the same material.

2.1 Aging range: a simple quench experiment

To determine the dielectric constant, we measure the complex impedance of a capacitor whose dielectric is the PMMA sample. In our experiment a disk of PMMA of diameter $10cm$ and thickness $0.3mm$ is inserted between the plates of a capacitor whose vacuum capacitance is $C_o = 230pF$ (see fig.1 for details). The capacitor is inside an oven whose temperature T may be changed from $300K$ to $500K$. The temperature stability is within $0.1K$. The maximum heating and cooling rate $|R| = |dT/dt|$ is about $180K/h$. We checked that the temperature difference between the two capacitor plates is always smaller than $1K$ both during the heating and the cooling cycles.

The capacitor is a component of the feedback loop of a precision voltage amplifier whose input is connected to a signal generator. We obtain the real and imaginary part of the capacitor impedance by measuring the response of the amplifier to a sinusoidal input signal. This apparatus allows us to measure the real and imaginary part of the dielectric constant $\epsilon = \epsilon_1 + i\ \epsilon_2$ as a function of temperature T, frequency f and time t. Relative variations of ϵ smaller than 10^{-3} can be measured in all the frequency range used in this experiment, i.e. $0.1Hz < f < 100Hz$. The following discussion will focus only on ϵ_1 (thus we will omit subscript 1), for which we have the best accuracy, but the behaviour of ϵ_2 leads to the same conclusions.

The measurement is performed in the following way. We first initialize the PMMA history by heating the sample at a temperature $T_{max} > T_g$. In this case the applied thermal cycle is that shown in fig.1(b). The sample is left at $T_{max} = 415K$ for a few hours, so that

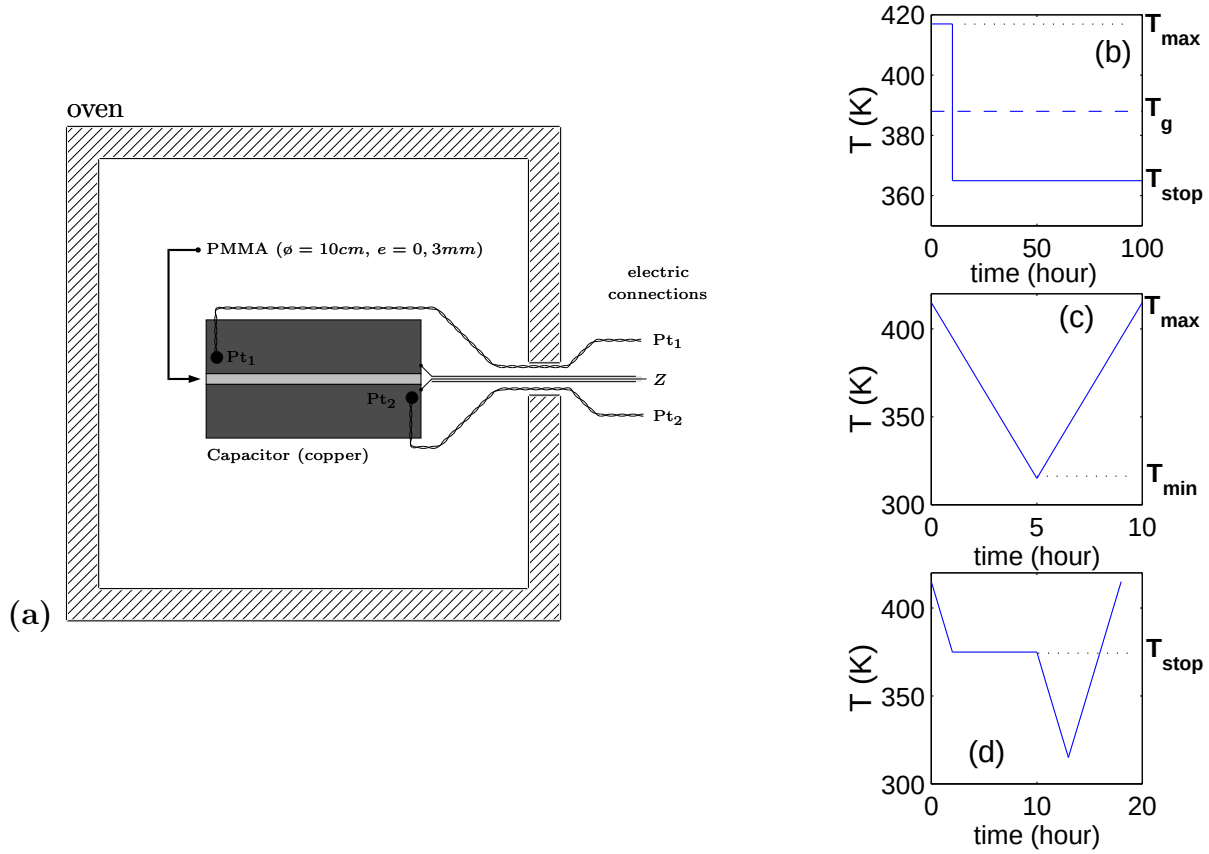

Figure 1: (a) **Experimental set-up for PMMA**. PMMA is the dielectric of a capacitor whose vacuum capacitance is $C_0 = 230pF$. This impedance Z is inside an oven which controls the temperature and acts like an electrical screen. The dielectric temperature is measured by two platinum probes (Pt). (b-d) **Typical thermal cycles applied to the sample**. (b) Temperature quench from above to below Tg. (c) Temperature ramp at constant cooling and heating rates. (d) Cooling stop for 10 *hours* at T_{stop}

equilibrium can be assumed for the initial condition. The temperature is rapidly decreased at $R = -180K/h$ to a temperature $T_{stop} < T_g$, where it is regulated by the oven. The zero of the aging time is taken at the instant, during the quench, when the sample temperature is equal to T_g. Typical aging curves of ϵ as a function of time are shown in fig.2, for different T_{stop} at $f = 1Hz$ and different f at $T_{stop} = 365K$. We clearly notice a logarithmic dependence on time of the dielectric constant as soon as the temperature is stabilized, in all the temperature and frequency range we have explored. However the aging curve depends on T_{stop} and f : the sample properties evolve faster when T_{stop} is close to T_g and f is small.

Specifically one can write $\epsilon(T_{stop}, t, f) = A(T_{stop}, f) - B(T_{stop}, f)\ \log(t/t_o)$ with $t_o = 1h$. Here A is the value of ϵ at $t = t_o$. It is found that A and B are functions of T_{stop} and of the frequency f at which the dielectric constant is measured. Note that as A and B depend also weakly on the cooling rate R, we always use $R = -180K/h$ in these experiments. The values of B, measured at $f = 1Hz$, are plotted in fig.3(a) as a function of T_{stop}. B is an increasing

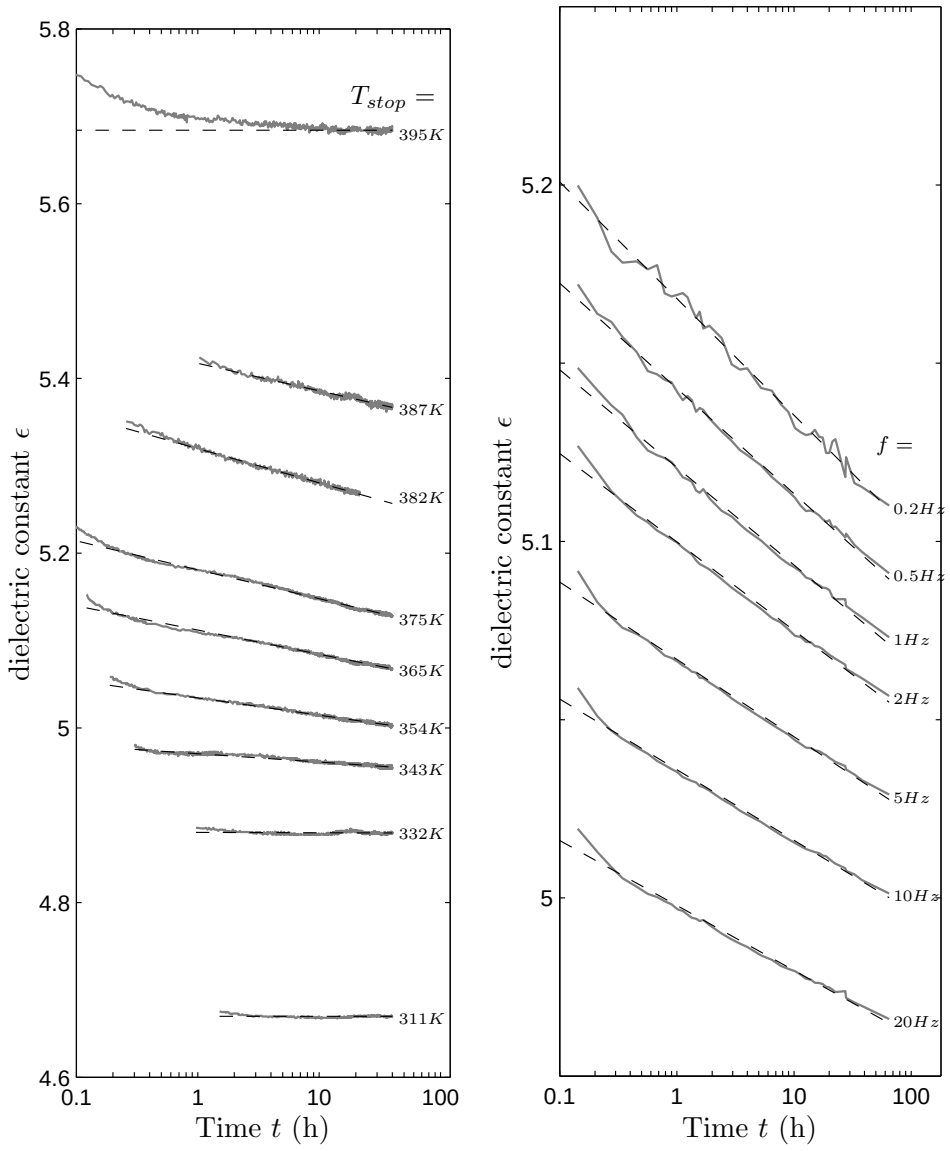

Figure 2: **Dependence on t of ϵ after a quench.** (a) Aging measured at $f = 1Hz$ after a quench at various T_{stop}. (b) Aging measured after a quench at $T_{stop} = 365K$ at various f. A logarithmic fit in time of all these curves is accurate as soon as temperature is stabilized, except for $T_{stop} = 395K > T_g$

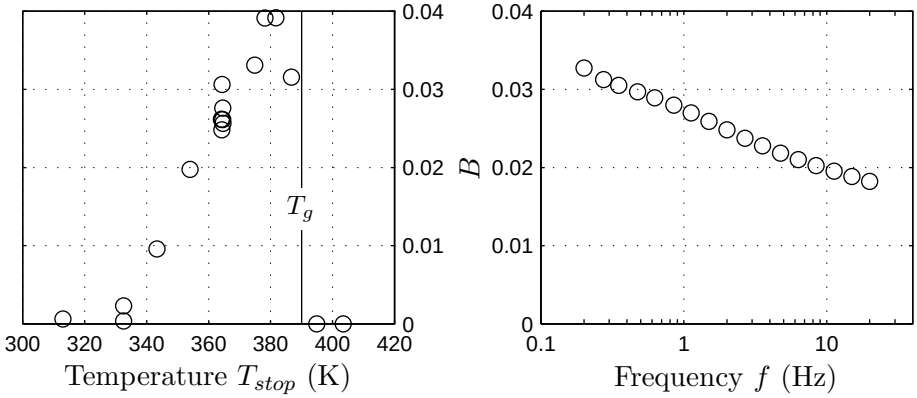

Figure 3: (a) **Dependence on** T_{stop} of B at $f = 1Hz$, where B is the parameter of the logarithmic fit of the dielectric constant $\epsilon(T_{stop}, t, f) = A(T_{stop}, f) - B(T_{stop}, f)\ \log(t/1h)$ after a quench at T_{stop}. (b) **Dependence on** f of B at $T_{stop} = 365K$.

function of T_{stop} till a temperature T_m close to T_g, but goes down to 0 if $T_{stop} > T_g$. Indeed for a quench temperature larger than T_g the sample can reach a thermodynamic equilibrium, so no aging is observed but only a relaxation of ϵ toward its stationary value. The long time behaviour is stationary and B goes to 0.

The values of B, measured at $T_{stop} = 365K$, are plotted in fig.3(b) as a function of f. B is a slowly increasing function for $f \to 0$. Indeed aging is smaller at high frequencies than at low frequencies (a theoretical justification of such a behaviour can be found for example in ref.[9]).

These curves determine the region where to work. In our dielectric measurement aging can be accurately observed between $335K$ and $T_g = 388K$. We will probe $f = 0.1Hz$ and $f = 1Hz$ where aging effects are the largest in our frequency range.

2.2 Memory and rejuvenation

2.2.1 Historical background

In spite of the interesting experimental [13]-[23] and theoretical progress [2, 9, 25], done in the last years, the physical mechanisms of aging are not yet fully understood. In fact on the basis of available experimental data it is very difficult to distinguish which is the most suitable theoretical approach for describing the aging processes of different materials. In order to give more insight into this problem several experimental procedures have been proposed and applied to the study of the aging of various materials, such as spin-glasses (SG)[13, 4, 16, 21, 22, 23], orientational glasses (OG)[14, 17], polymers [1, 18, 45, 20, 26] and supercooled liquids (SL)[15].

The very well known Kovacs [26] experiment was probably among the first in showing that the state of a glass is strongly determined by its thermal history. In the Kovacs experiment the material is submitted to the following temperature cycle sketched in the insert of fig.4(a). The material is rapidly quenched from the liquid at a temperature T_o to the glass phase at a temperature T_1 at which the volume of the glass is V_1. The material is maintained at T_1

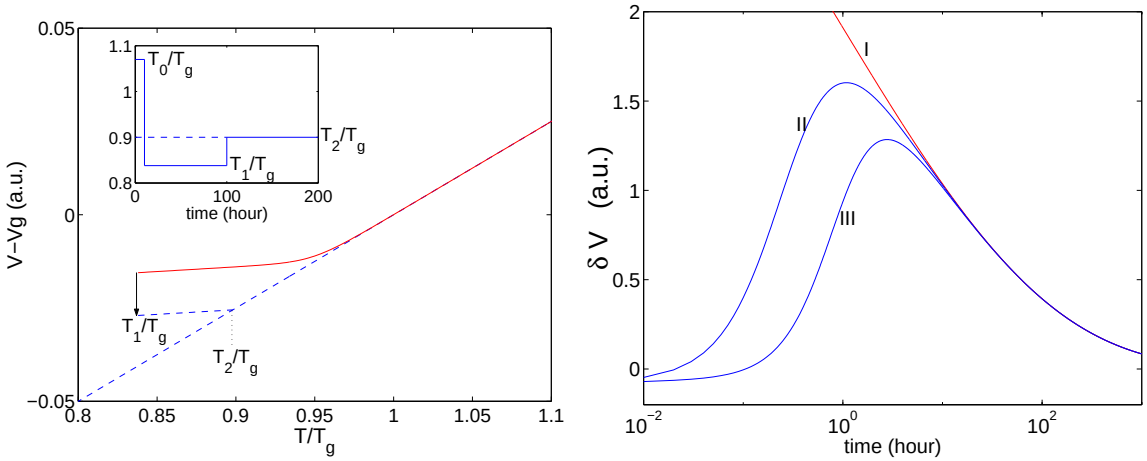

Figure 4: **Kovacs's experiment**.(a) Volume of a sample versus temperature during a quench from a temperature $T_o > T_g$ to a temperature $T_1 < T_g$. The sample is aged about 100 hours at T_1 and volume decreases from V_1 to V_2. The temperature is then changed to T_2 at which V_2 is the equilibrium volume. In the insert we sketch the sample temperature as a function of time. (b) Time evolution of $\delta V = V - V_2$ when the sample is directly quenched from T_o to T_2 (curve I) and when the temperature is changed from T_1 to T_2 (curves II and III) for two different T_1. The amplitude of the peak increases by increasing the difference $T_2 - T_1$.

for about 100 hours. Because of aging the volume of the material decreases as a function of time going from V_1 to V_2, as shown in fig.4(a). Then the material is rapidly heated at a temperature T_2 at which V_2 is the equilibrium volume. One could think that no appreciable evolution appears as a function of time. Instead the time evolution of the sample volume at temperature T_2, sketched in fig.4(b), is quite different. The volume first increases, reaches a maximum and then decreases to reach again the value V_2. As shown in fig.4(b), the amplitude of the maximum depends of course on T_1 and on the waiting time at T_1. Figure fig.4(a) points out the difference between the time evolution of the volume after a quench from T_o to T_2 and after the aging at T_1. Another example of history dependent effect is that induced by the aging at low temperature, known as prepeak in polymer literature [18]. Such an aging does not produce important changes in the enthalpy. However when increasing temperature, a peak in the curve of the heat capacity versus temperature is observed at a temperature close to T_g.

Other procedures were proposed for spin glasses and applied to other materials. Among these procedures we may recall the applications of small temperature perturbations to a sample during the aging time [13, 14, 15, 45]. One of the main results of these experiments is that the time spent at low enough temperature does not contribute to the aging behaviour at the higher temperature. Most surprisingly, the aging at low temperature is independent on the aging at an higher temperature. In order to have a better understanding of the free energy landscape of SG and OG, a very smart protocol has been proposed [4] and used in several experiments [4, 16, 17]. This protocol, which is characterized by a temporary cooling

stop, has revealed that in SG and in OG the low temperature state is independent of the complete cooling history (*Rejuvenation*) but that these materials keep the memory of all the aging history (*Memory effect*) [4]. In the next section we describe in some details the application of this procedure to the aging of PMMA.

As we already mentioned, several kinds [18, 26] of "memory effects" for polymers have been described in literature. The most famous one is that of Kovacs [26]. However the thermal cycles used in these experiments are quite different from those proposed in [4]. Thus it is interesting to check how polymers behave when they are submitted to this new thermal procedure, which can give new insight on the aging of these materials. Moreover, the use of the same protocols makes the comparison between different kinds of glasses easier.

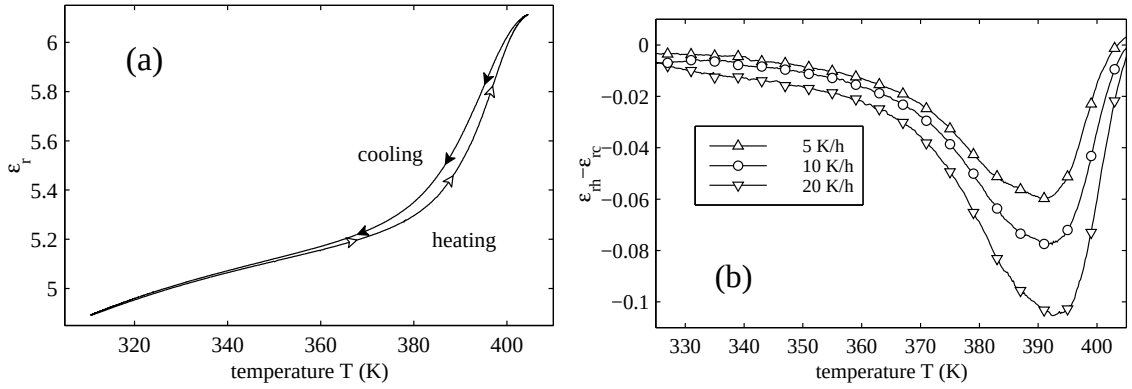

Figure 5: (a) **Evolution of ϵ_r at $f = 0.1Hz$ as a function of T.** Reference curve obtained with $|R| = 20K/h$. (b) **Hysteresis of the reference curve** (difference between the heating and cooling curves $\epsilon_{rh} - \epsilon_{rc}$) for 3 different $|R|$: $5K/h$ ($\triangle$), $10K/h$ ($\circ$) and $20K/h$ ($\triangledown$).

2.2.2 Memory experiment on PMMA

We describe experiments following the protocol first proposed in ref.[4]: a temporary stop is done during the cooling of the sample, and its consequence on the dielectric constant behaviour are studied. The measurement is performed in the following way: the PMMA history is first reinitialized by heating the sample at a temperature $T_{max} > T_g$ and leaving it at $T_{max} = 415K$ for a few hours. Then it is slowly cooled from T_{max} to a temperature $T_{min} = 313K$ at the constant rate R and heated back to T_{max} at the same $|R|$. The dependence of ϵ on T obtained by cooling and heating the sample at a constant $|R|$ (temperature time evolution of fig.1(c), is called the reference curve ϵ_r).

As an example of reference curve we plot in fig.5(a) ϵ_r, measured at $0.1Hz$ and at $|R| = 20K/h$. We see that ϵ_r presents a hysteresis between the cooling and the heating in the interval $350K < T < 405K$. This hysteresis depends on the cooling and heating rates. Indeed, in fig.5(b), the difference between the heating curve (ϵ_{rh}) and the cooling curve (ϵ_{rc}) is plotted as a function of T for different $|R|$. The faster we change temperature, the bigger hysteresis we get. Furthermore the temperature of the hysteresis maximum is a few degrees above T_g, specifically at $T \approx 392K$. The temperature of this maximum gets closer to T_g

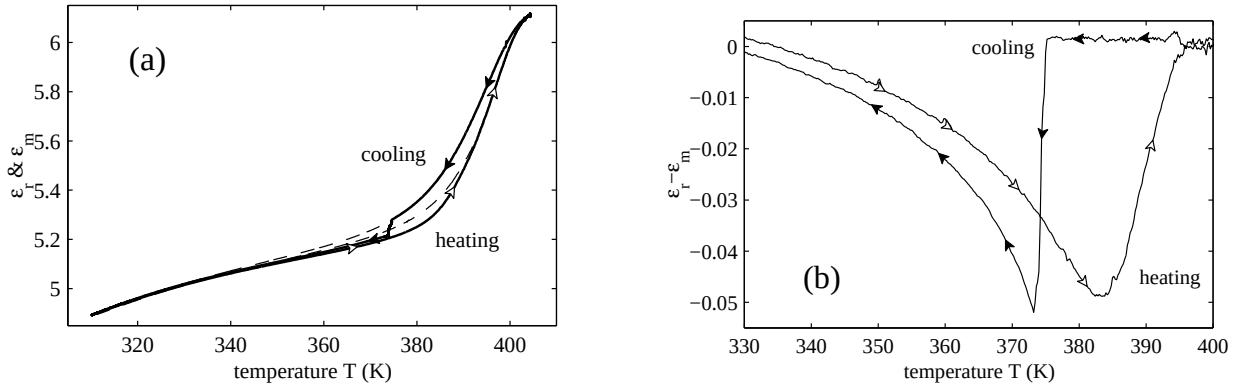

Figure 6: **Memory effect** (a)Evolution of ϵ at $f = 0.1Hz$ as a function of T. The dashed line corresponds to the reference curve (ϵ_r) of Fig.5(a). The solid bold line corresponds to a different cooling procedure: the sample is cooled, at $R = -20K/h$, from T_{max} to $T_{stop} = 374K$, where cooling is stopped for $10h$. Afterwards the sample is cooled at the same R till T_{min} and then heated again at $R = 20K/h$ till T_{max}. (b) Difference between the evolution of ϵ_r and ϵ_m. Downward filled arrows correspond to cooling ($\epsilon_{mc} - \epsilon_{rc}$) and upward empty arrows to heating ($\epsilon_{mh} - \epsilon_{rh}$).

when the rate is decreased. We neglect for the moment the rate dependence of the hysteresis and we consider as reference curve the one, plotted in fig.5(a), which has been obtained at $f = 0.1Hz$ and at $|R| = 20K/h$. The evolution of ϵ can be quite different from ϵ_r if we use the temperature cycle proposed in ref.[4] and shown in fig.1(d). After a cooling at $R = -20K/h$ from T_{max} to $T_{stop} = 374K$ the sample is maintained at T_{stop} for $10h$. After this time interval the sample is cooled again, at the same R, down to T_{min}. Once the sample temperature reaches T_{min} the sample is heated again at $R = 20K/h$ up to T_{max}. The dependence of ϵ as a function of T, obtained when the sample is submitted to this temperature cycle with the cooling stop at T_{stop}, is called the memory curve ϵ_m. In fig.6(a), ϵ_m (solid line), measured at $f = 0.1Hz$, is plotted as a function of T. The dashed line corresponds to the reference curve of fig.5(a). We notice that ϵ_m relaxes downwards when cooling is stopped at T_{stop}: this corresponds to the vertical line in fig.6(a) where ϵ_m departs from ϵ_r. When cooling is resumed ϵ_m merges into ϵ_r for $T < 340K$. The aging at T_{stop} has not influenced the result at low temperature. This effect has been called *rejuvenation* in recent papers [22].

During the heating period the system reminds the aging at T_{stop} (cooling stop) and for $340K < T < 395K$ the evolution of ϵ_m is quite different from ϵ_r. In order to clearly see this effect we divide ϵ_m in the cooling part ϵ_{mc} and the heating part ϵ_{mh}. In fig.6(b) we plot the difference between ϵ_m and ϵ_r. Downward filled arrows correspond to cooling ($\epsilon_{mc} - \epsilon_{rc}$) and empty upward arrows to heating ($\epsilon_{mh} - \epsilon_{rh}$). The difference between the evolutions corresponding to different cooling procedures is now quite clear. The system reminds its previous aging history when it is reheated from T_{min}. The amplitude of the memory corresponds well to the amplitude of the aging at T_{stop} but the temperature of the maximum is shifted a few degrees above T_{stop}. On fig.7 we show that this temperature shift is independent of T_{stop} for temperatures where aging can be measured in a reasonable time

(above $335K$). In contrast the amplitude of the downward relaxation at T_{stop} is a decreasing function of T_{stop}, as expected from the first section measurements: no aging can be measured at $T_{stop} < 335K$ (see fig.3(a)).

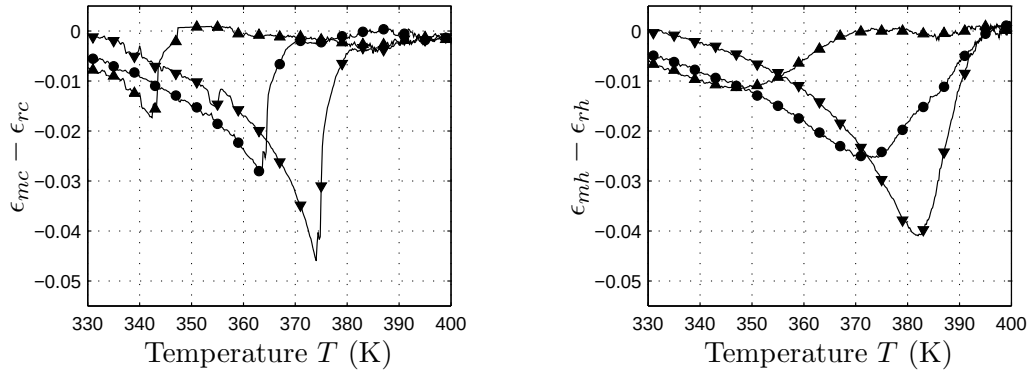

Figure 7: **Dependence on T_{stop}.** Difference between ϵ_r and ϵ_m for 3 different cooling stops measured at $f = 0.1Hz$ for $|R| = 10K/h$ and $t_{stop} = 10h$. (a) Writing memory (cooling): $\epsilon_{mc} - \epsilon_{rc}$ with $T_{stop} = 344K$ (▲), $364K$ (●) and $374K$ (▼). (b) Reading memory (heating): $\epsilon_{mh} - \epsilon_{rh}$ (same symbols as in (a)).

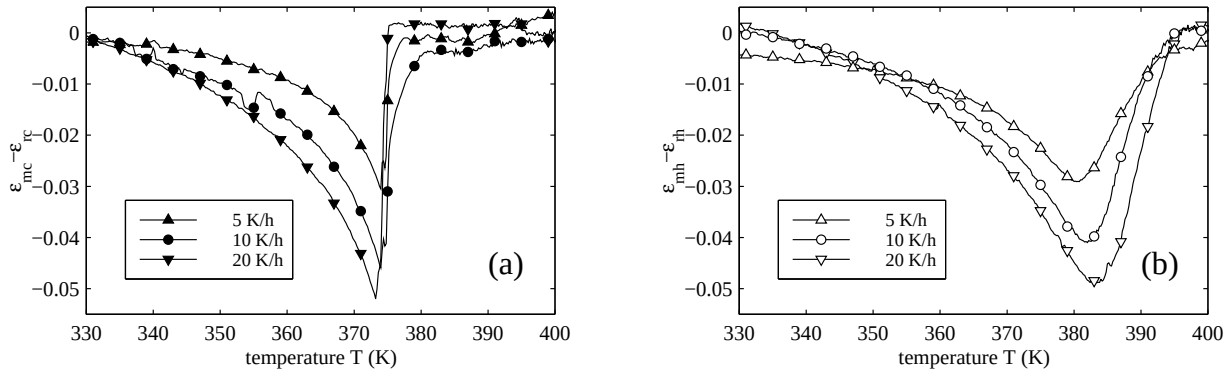

Figure 8: **Dependence on the cooling and heating rate.** Difference between ϵ_r and ϵ_m (aging at $T_{stop} = 374K$ for $10h$) measured at $f = 0.1Hz$ for 3 $|R|$. (a) Writing memory (cooling): $\epsilon_{mc} - \epsilon_{rc}$ at $5K/h$ (▲), $10K/h$ (●) and $20K/h$ (▼). (b) Reading memory (heating): $\epsilon_{mh} - \epsilon_{rh}$ at $5K/h$ (△), $10K/h$ (○) and $20K/h$ (▽).

This memory effect seems to be permanent because it does not depend on the waiting time at T_{min}. Indeed we performed several experiments in which we waited till $24h$ at T_{min}, before restarting heating, without noticing any change in the heating cycle. In contrast the amplitude and the position of the memory effect depend on R and on the measuring frequency. As expected from the measurements of section(2.1), the higher is the frequency, the smaller is the downward relaxation, so the smaller is the memory effect. Furthermore the faster is the rate $|R|$, the larger is the downward relaxation of the dielectric constant during

the cooling stop. As the amplitude of the memory effect is equal to that of the relaxation, we just expect the memory effect to increase with $|R|$. But as we can see on fig.8, the temperature positions of the maxima are rate dependent too: the larger is $|R|$, the farther the temperature of the maximum is shifted above the aging temperature T_{stop}. The cooling rate is not the only control parameter of the memory effect, the heating rate is relevant too.

2.2.3 Advanced memory experiments

In this section we apply to the PMMA sample more complicated temperature histories (inspired from spins glasses experiments [4, 21]): What happens if we try to read a memory twice ? If we make two cooling stops ?

2.2.4 Deleting memory

In this experiment, we show that a memory can be read only one single time: reading a memory effect also deletes it. This experiment is inspired from similar ones done in spin glasses [21]. First we follow the classic procedure described in the previous section: during the cooling ramp at $R = -20K/h$, a temporary stop is done for $t_{stop} = 20h$ at $T_{stop} = 345K$, and then heating the sample from T_{min} with the same $|R|$. In fig.9(a) we plot the difference between the heating branches of ϵ_m and ϵ_r measured at $f = 0.1Hz$. The departure from the reference curve above T_{stop} when lowering temperature is due to a smooth cutting of cooling, but this imperfection has no detectable effect on the heating curve. We can follow the memory of the cooling stop at T_{stop}, and when the memory curve almost merges the reference one, for $T_i = 368K$, we quickly stop heating and resume cooling at $R = -20K/h$. Notice that this inversion temperature T_i is smaller than T_g, which means that the sample has not been reinitialized. When T_{min} is reached again, we make a classic heating at $R = +20K/h$ (see the temperature history of the sample in the inset of fig.9(a)).

This second heating curve is really different from the first one: there are no tracks of the cooling stop at $T_{stop} = 345K$, but something like the memory of a stop around $370K$. What we see now is in fact only the memory of the stop at T_i: as the sample stays a few minutes around T_i (the time needed to inverse R to $-R$), it ages a little at T_i and we find a memory of this event. This can be checked on fig.9(b), where we only show the memory of the inversion at the same temperature T_i, without the first memory. The curves corresponding to the second heating are exactly the same for the two experiments, showing that the first heating deletes all information about temperatures lower than T_i, even though $T_i < T_g$.

2.2.5 Double memory

More insight on the properties of the memory effects can be obtained by submitting the sample to a more complex cooling procedure consisting of two cooling stops. This procedure, which has been called the double memory effect, has been carried out successfully in spin glasses [4] where it has been observed that if two stops are done during cooling, the heating curve will present a memory effect for both stops. The difficulty that arise when trying to reproduce this experiment in PMMA is the narrowness of the aging range: when cooling the sample under T_{stop}, ϵ_m rejoins the reference curve only for temperatures where aging almost

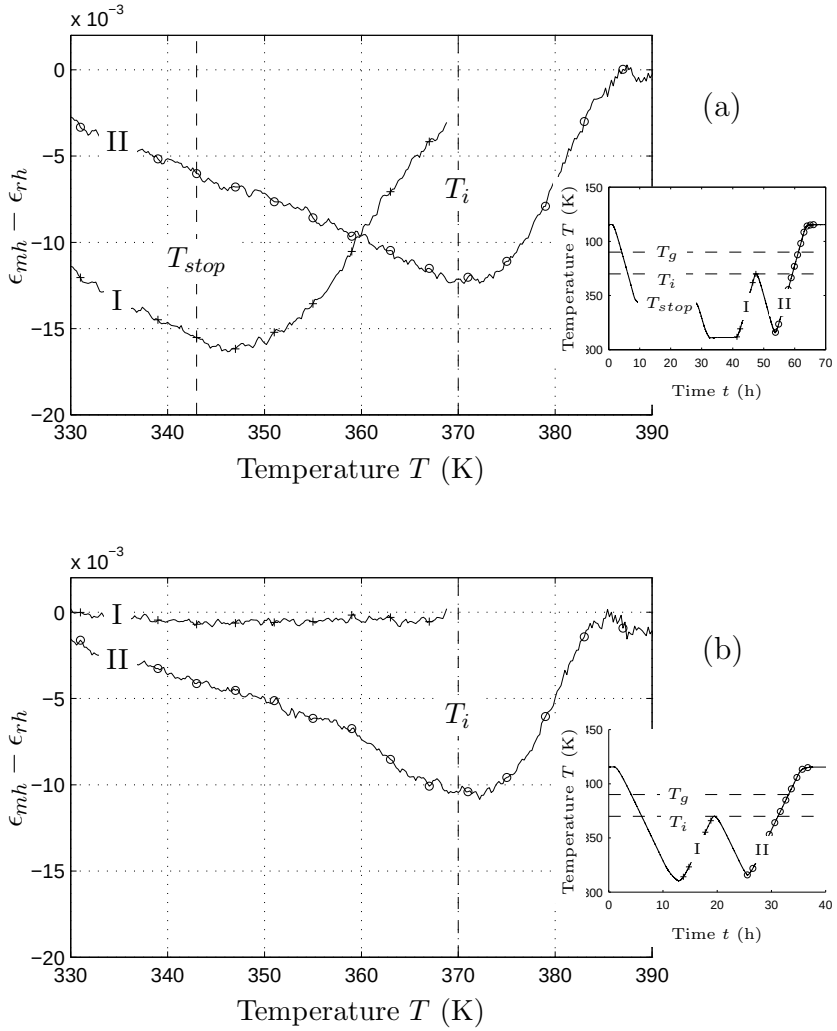

Figure 9: **Deleting a memory by reading it.** (a) Difference between heating curves ϵ_{rh} and ϵ_{mh} after the temperature history shown in the inset: after a classic reading the memory of a $20h$ stop at $T_{stop} = 345K$ with $|R| = 20K/h$ and $f = 0.1Hz$ (+), the sample is cooled again when the temperature reaches $T_i < T_g$. The second reading ($\circ$) is very different since no tracks of T_{stop} is found but a sort of memory of the inversion temperature T_i. This can be checked on (b), where we only test the memory of the inversion. The difference between the second heating curves ($\circ$) $\epsilon_{mh} - \epsilon_{rh}$ is exactly the same for both temperature histories. Heating the sample up to T_i reinitializes the lower temperature behaviour, even though $T_i < T_g$.

vanishes. It is therefore difficult to record two well distinct cooling stops. This is illustrated in fig.10, where $T_{stop1} = 375K$ and $T_{stop2} = 345K$: ϵ_m has not completely merged into ϵ_r when we stop cooling for the second time.

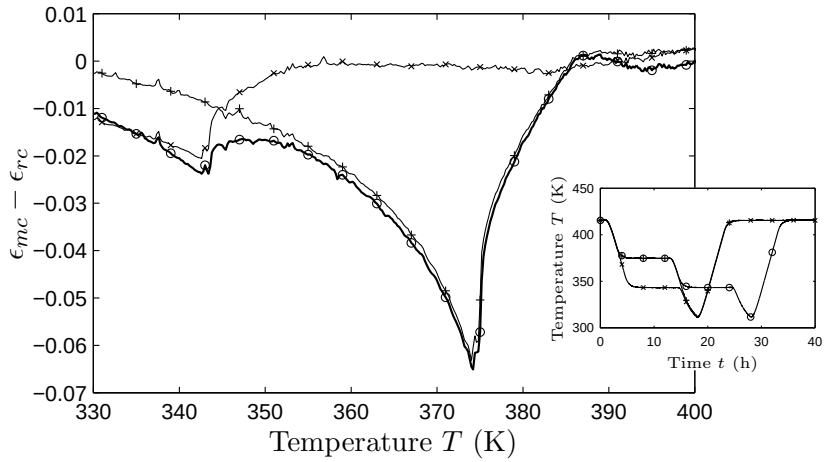

Figure 10: **Double memory recording.** Difference between cooling curves ϵ_{mc} and ϵ_{rc} during the temperature history shown in the inset, for $|R| = 20K/h$, and $f = 0.1Hz$: one $10h$ stop at $T_{stop1} = 375K$ (+), one $10h$ stop at $T_{stop2} = 345K$ (x), and two $10h$ stops at $T_{stop1} = 375K$ and $T_{stop2} = 345K$ (∘). The low temperature state is independent of high temperature history: aging during $10h$ at T_{stop2} produces the same relaxation, whatever happened before at higher temperatures.

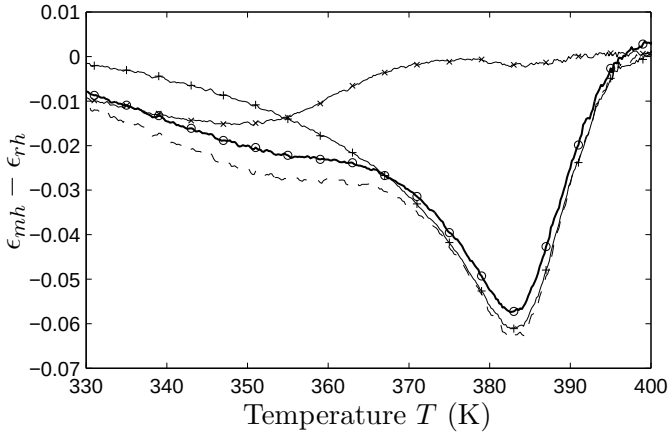

Figure 11: **Double memory reading.** Difference between heating curves ϵ_{mh} and ϵ_{rh} corresponding to the cooling curves of fig.10: reading of a single stop at $T_{stop1} = 375K$ (+) and $T_{stop2} = 345K$ (x), reading of a double stop at T_{stop1} and T_{stop2} (∘). The dashed line is the sum of the two single stop curves, it is a very good approximation of the double memory reading. Memory effects thus appear only additive in this case, where T_{stop1} and T_{stop2} are sufficiently far from each other.

The double memory experiments allow us to point out another important property of PMMA aging: when temperature is lowered after the first stop, the system not only recover the same value of ϵ, but also the same aging properties. Indeed, a $10h$ stop at $345K$ produces the same downward relaxation of ϵ, whatever the previous history is. The low temperature state is thus completely uninfluenced by the high temperature history.

If we now heat the sample after the two cooling stops, we obtain the bolt curve of fig.11. If the memory of T_{stop1} is obvious, the lower temperature stop at T_{stop2} must be hidden in the first part of the curve. In order to check the presence of the memory effect of the second stop, let us suppose that this effect is just additive, that is the memory of a double stop is just the sum of the memory of both individual stops if their temperature is sufficiently different. So we plot with a dashed line in fig.11 the sum of the single memories of T_{stop1} and T_{stop2}. Within errors bars, the two curves are the same, so we conclude that even if the memory effects overlap in the narrow aging range of PMMA, double memory experiments also work in this polymer.

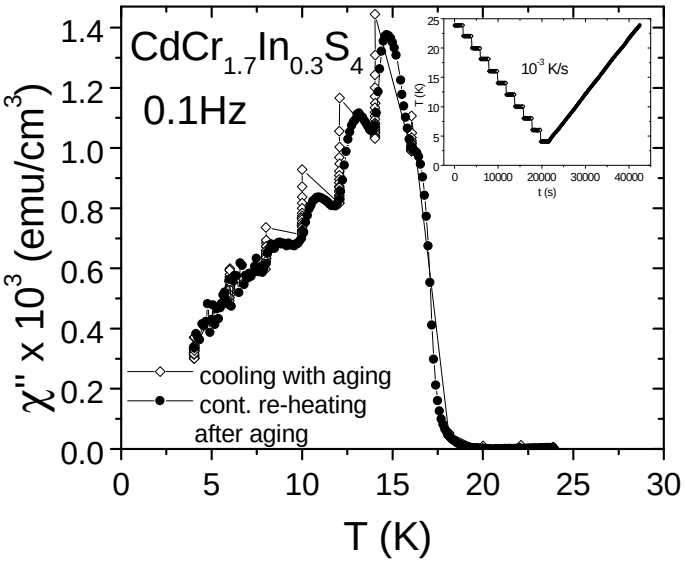

Figure 12: **Memory and rejuvenation in a spin glass.** Multiple memories on the magnetic susceptibility, measured at $0.1Hz$, of a spin glass. The sample has been cooled by successive stops (see insert for the temperature history) and heated at constant rate. At each cooling stop the sample ages (downward relaxation). During heating the sample remembers all the cooling stops.(see text for details)

2.2.6 Direct comparison with the memory effects in spin-glasses

In the previous section we have described the behaviour of a PMMA sample submitted to the same temperature cycle used to study memory and rejuvenation effects in various kinds of spin glasses and in orientational glasses. Our dielectric measurements clearly show the presence of rejuvenation and memory in PMMA. However these effects are less strong in PMMA than in spin-glasses. In order to stress this difference we consider the results of an

experiment performed by V. Dupuis, on a spin glass $CdCr_{1.7}In_{0.3}S_4$ with $T_g \simeq 17K$ [23, 24]. One of the main results of this experiment is shown in fig.12, which has been kindly given to us by E. Vincent. The temperature cycle applied to the sample is sketched in the insert. The sample is heated at 25K and then cooled by steps of 2K till 3K. It is then heated again at a constant rate till 25K. Between two successive cooling steps the temperature is kept constant for $2000s$. During this temperature cycle the magnetic susceptibility is measured at a frequency of $0.1Hz$. The imaginary part χ'' of the magnetic susceptibility is plotted in fig.12 as a function of temperature. The open symbols correspond to cooling and the filled symbols to heating. The isothermal aging is observed on the downward relaxation at each temperature plateau. At the same time we see that a cooling step produces an upward jump of χ'' and a restart of aging: this is the rejuvenation effect. When the sample is heated again, χ'' presents minima exactly at the temperatures where the sample was aged during the cooling: this is the memory effect.

Comparing fig.12 with the results on PMMA, described in the previous section, we immediately notice that there are analogies but very important differences. We clearly see that the SG has no hysteresis and the memory effect occurs at the same temperature of the cooling stops. Most importantly multiple stops are quite well remembered by the SG, whereas are weakly seen in PMMA.

2.3 Discussion on the memory effect

As we already mentioned in sect.(2.2.1) the observation of a memory of the thermal history in polymers is not new and various thermal protocols have been used to show this effect. The thermal protocol described in sect.(2.2) of this lecture is the same used to study aging phenomena in SG and OG. Thus the application to a polymer glass of the same procedure used in OG and SG allows us to address the question of the universality of the memory and rejuvenation phenomena in different materials. This is a very important point in order to understand whether the same theoretical approach can be used to describe aging phenomena in different materials.

Let us summarize the main results of these low frequency dielectric measurements on PMMA:

a) The reference curve ϵ_r, obtained at constant cooling and heating rate $|R|$ is hysteretic. This hysteresis is maximum a few degrees above T_g.

b) The hysteresis of ϵ_r increases with $|R|$.

c) Writing memory: a cooling stop produces a downward relaxation of ϵ_m. The amplitude of this downward relaxation depends on T_{stop} and it decreases for decreasing T_{stop}. It almost disappears for $T_{stop} < 335K$.

d) When cooling is resumed ϵ goes back to the cooling branch of the reference curve. This suggests that the low temperature state is independent on the cooling history.

e) Reading memory: upon reheating ϵ_m reminds the aging history and the cooling stop (*Memory*). The maximum of the memory effect is obtained a few degrees above T_{stop}.

f) The memory effect does not depend on the waiting time at low temperature but it depends both on the cooling and heating rates. The memory effect increases with $|R|$.

g) Double memory effects are observed with more difficulty in PMMA than in SG. The difference comes from the fact that aging effects are reduced when temperature is lowered. However a careful analysis of experimental data allows us to show the existence of double memory effects in PMMA.

h) The memory effect is deleted by a reading, even if the temperature remains smaller than T_g.

It is interesting to discuss the analogies and the differences between this experiment and similar ones performed on SG [4, 16, 22, 23] and on OG [17]. It turns out that, neglecting the hysteresis of the reference curve of PMMA and of OG, the behaviour of these materials is quite similar to that of SG. A strong rate dependence has been observed in Ising spin-glasses too [22]. During the heating period PMMA, SG and OG remember their aging history, although the precise way, in which history is remembered, is material dependent. Furthermore in these materials the low temperature state is independent on the cooling history. One can estimate the temperature range δT where the material response is different from that of the reference curve because of the cooling stop. It turns out that the ratio $\delta T/T_G$ is roughly the same in PMMA, in SG and in OG, specifically $\delta T/T_G \simeq 0.2$. The important difference between SG and PMMA is in the dependence on T_{stop} of the amplitude of the downward relaxation: it is strong in PMMA and weak in SG (compare fig.12 with figs.10,11).

Our results seem to indicate that memory and rejuvenation phenomena in the aging process may be described by models based on a hierarchical free energy landscape, whose barriers grow when temperature is lowered [13, 4]. However the dependence of the memory effect on $|R|$ and the independence on the waiting time at T_{min} mean that, at least for PMMA, the free energy landscape has to depend not only on temperature but also on $|R|$. Many models [6, 7, 9, 13, 27] and numerical simulations [38, 40] do not take into account this dependence because they consider just a static temperature after a quench. In contrast point f) indicates that the cooling history is relevant too.

These difficulties can be avoided if one considers models based on a slow domain growth and domain walls reconformations in the pinning field created by disorder (see for example ref.[25] and references therein). These models imply the existence of a hierarchy of length scales l with a characteristic time $\tau \propto l^z$. Recent numerical simulations [28] show that this is an important ingredient in order to have memory/rejuvenation effects. However one of the drawbacks of such a model is that memory is recovered only if the time spent at low temperature is short enough [25]. This effect does not seem to be true for PMMA and other materials at least on reasonable laboratory time scales.

As a conclusion the "memory" and rejuvenation effects seem to be two universal features of aging whereas the hysteresis is present in PMMA and in OG but not in all kinds of spin glasses. It would be interesting to know whether these effects are observed in other polymers and in supercooled liquids. These measurements show that many features of aging seem to be "universal" in several materials and that models based on spin glasses may be useful to describe aging in polymeric materials.

3 Effective Temperature of an aging material

The experimental procedures described in the previous section have been extremely useful to fix several constraints for the phenomenological models [6, 7], but these procedures are mainly based on the study of the response of the system to an external perturbation. Therefore they are unable to give informations on the system dynamics. Therefore, from an experimental point of view, it is extremely important to study not only the response of the system but also its thermal fluctuations. The analysis of thermal fluctuations is related also to another important aspect of aging dynamics, that is the definition of the temperature. Recent theories [11, 30] based on the description of spin glasses by a mean field approach proposed to extend the concept of temperature using a Fluctuation Dissipation Relation (FDR) which generalizes the Fluctuation Dissipation Theorem (FDT) for a weakly out of equilibrium system (for a review see ref. [9, 10, 11]).

In order to understand this generalization, we recall the main consequences of FDT in a system which is in thermodynamic equilibrium. We consider an observable V of such a system and its conjugate variables q . The response function $\chi_{Vq}(\omega)$, at frequency $f = \omega/2\pi$, describes the variation $\delta V(\omega)$ of V induced by a perturbation $\delta q(\omega)$ of q, that is $\chi_{Vq}(\omega) = \delta V(\omega)/\delta q(\omega)$. FDT relates the fluctuation spectral density of V to the response function χ_{Vq} and the temperature T of the system:

$$S(\omega) = \frac{2k_B\ T}{\pi\omega} Im\left[\chi_{Vq}(\omega)\right] \tag{1}$$

where $S(\omega) =< |V(\omega)|^2 >$ is the fluctuation spectral density of V, k_B is the Boltzmann constant, $Im\left[\chi_{Vq}(\omega)\right]$ is the imaginary part of $\chi_{Vq}(\omega)$. Textbook examples of FDR are Nyquist's formula relating the voltage noise to the electrical resistance and the Einstein's relation for Brownian motion relating the particle diffusion coefficient to the fluid viscosity [31].

When the system is not in equilibrium FDT, that is eq.1, may fail. For example violations, of about a factor of 2, of eq.1 have been observed in the density fluctuations of polymers in the glassy phase [32]. The first to propose that the study of the FDT violations are relevant for glassy systems was Sompolinsky [33]. This idea, which was generalized in the context of weak turbulence [34], has been reconsidered by Cugliandolo and Kurchan [11, 30] and successively tested in many analytical and numerical models of glass dynamics ([10],[35]-[41]) and in a few experiments.

Let us briefly recall the main and general findings of these models, which are very well described in this prooceedings in the Cugliandolo lecture [11]. Because of the slow dependence on t_w of the response functions, it has been proposed to use an FDR which generalizes eq.1 and which can be used to define an effective temperature $T_{eff}(\omega, t_w)$ of the system [10, 11]:

$$T_{eff}(\omega, t_w) = \frac{S(\omega, t_w)\ \pi\omega}{Im\left[\chi_{Vq}(\omega, t_w)\right]\ 2k_B} \tag{2}$$

In the time domain the effective temperature is usually defined by means of correlation functions $C(t, t_w)$ (Fourier transform of $S(\omega, t_w)$) and integrated response $R(t, t_w)$ (Fourier transform of $\chi_V q(\omega, t_w)$) [11]:

$$T_{eff}(t,t_w) = \frac{-C(t,t_w) + C(t_w,t_w)}{k_B\ R(t,t_w)} \tag{3}$$

It is clear that if eq.1 is satisfied $T_{eff} = T$, otherwise T_{eff} turns out to be a decreasing function of t_w and ω. The physical meaning of eq.2 is that there is a time scale (for example t_w), which allows one to separate the fast processes from the slow ones. In other words the low frequency modes, such that $\omega t_w < 1$, relax towards the equilibrium value much slower than the high frequency ones which rapidly relax to the temperature of the thermal bath. Therefore it is conceivable that the slow frequency modes keep memory of higher temperatures for a long time and for this reason their temperature should be higher than that of the high frequency ones. This striking behavior has been observed in several models of aging ([10],[35]-[41]). Further analytical and numerical studies of simple models show that eq.2 is a good definition of temperature in the thermodynamic sense [11, 10]. In spite of the large amount of theoretical studies there are only a few experiments where FDR is studied in aging materials. The experimental analysis of the dependence of $T_{eff}(\omega, t_w)$ on ω and t_w is very useful to distinguish among different models of aging because the FDT violations are model dependent ([10],[35]-[41]). Furthermore the direct analysis of the noise signal allows one to understand if the dynamics is either intermittent or continuous in time. this is another important characteristic of the aging models. Let us consider for example the trap model [6] which is based on a phase space description. Its basic ingredient is an activation process and aging is associated to the fact that deeper and deeper valleys are reached as the system evolves [8]. The dynamics in this model has to be intermittent because either nothing moves or there is a jump between two traps. This contrasts, for example, with mean field dynamics which is continuous in time [30]. This is not the only difference because in the trap model T_{eff} depends on the observable whereas it is observable independent in mean field model [8, 42].

FDT violations in aging materials have been measured just in a few experiments ([44],[45, 46], [47, 48], [49]). In the next sections we will first describe the x-ray experiment where the violation of FDT have been first observed and we will describe the reasons why these measurements are not sufficient to test FDR. We then briefly analyze another experiment [44] where FDR has been studied in some details. This is a single frequency experiment and thus T_{eff} is not completely characterized. For this reason we summarize the main results of two experiments where the FDT violation has been studied in the dielectric measurements of a gel [45, 46], during the sol-gel transition, and of a polymer, after a quench. In both cases the effective temperature defined using eq.2 is huge and the persistent time of the violation is extremely long. We have therefore analyzed directly the time evolution of the noise signal in both experiments and we find a strongly intermittent behaviour in both materials. In this lecture we will describe the main results of this analysis and we want also to point out the common features observed in the slow relaxation dynamics of these two materials.

In the case of the gel we want to address another important question. Specifically we have analyzed whether T_{eff} does depend on the couple of conjugated variables used in the measure of FDR. This is actually another important information because this dependence of T_{eff} on the observables is not the same in all the models [11, 42].

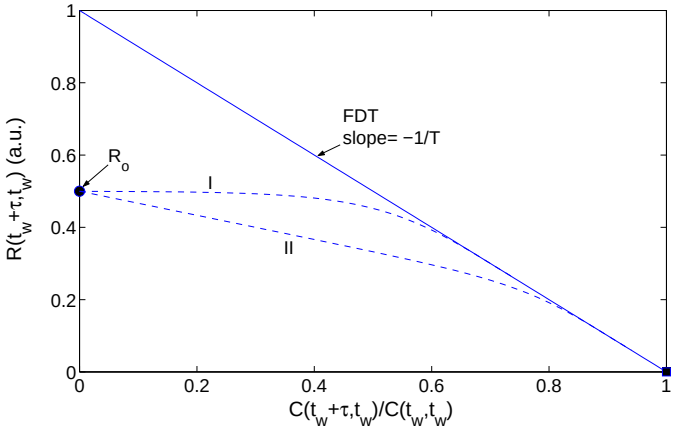

Figure 13: **Xray experiment** Schematic drawing of the response versus correlation. The response is in this case the isothermal compressibility and the correlation is given by the density fluctuations. The continuous straight line of slope $1/T$ is the prediction of FDT in this plot. See text for more details.

3.1 The x-ray scattering experiment

The violation of the FDT in aging polymers was already pointed out by Wendorff and Fisher [32]. Indeed in a x-ray scattering experiment, the intensity $I(0)$ of scattered x-rays at small angles is related to the density fluctuations $\delta\rho$:

$$\frac{<\delta\rho^2>}{\rho^2} \propto I(o) \tag{4}$$

From FDT one finds:

$$<\delta\rho^2> \;=\; \frac{K_B\ T\ \rho^2\chi_T}{V} \tag{5}$$

where χ_T is the isothermal compressibility of the polymer under study. They separately measured χ_T by standard techniques and $<\delta\rho^2>$ by x-ray scattering. Weandorf and Fisher found that eq.5 was satisfied by standard liquids, whereas a violation between 2.5 and 5 of eq.5 was observed for various polymers. Although this measurement is a strong indication that FDT is violated in an aging polymer, it is not very useful to know the behaviour of $T_{eff}(t,t_w)$ and to compare it with theoretical models. Indeed to compare with theory one has to consider the equation [11]:

$$-C(t_w+\tau,t_w)+C(t_w,t_w) = K_B\ T_{eff}(t,t_w)\ R(t_w+\tau,t_w) \tag{6}$$

In order to construct $T_{eff}(t,t_w)$ one has to measure, as a function of t_w and τ, both the correlation $-C(t_w+\tau,t_w)$ of the density fluctuations and the integrated response $R(t_w+\tau,t_w)$,that is the isothermal compressibility. Eq.5 is just the limit for $\tau\to\infty$ of eq.6, that is $\lim_{\tau\to\infty} C(t_w+\tau,t_w)=0$ and $\lim_{\tau\to\infty} R(t_w+\tau,t_w)=R_o$. Thus only two points are available on the plane $(C(t_w+\tau,t_w),R(t_w+\tau,t_w))$, specifically the point $(C(t_w,t_w),0)$, obtained

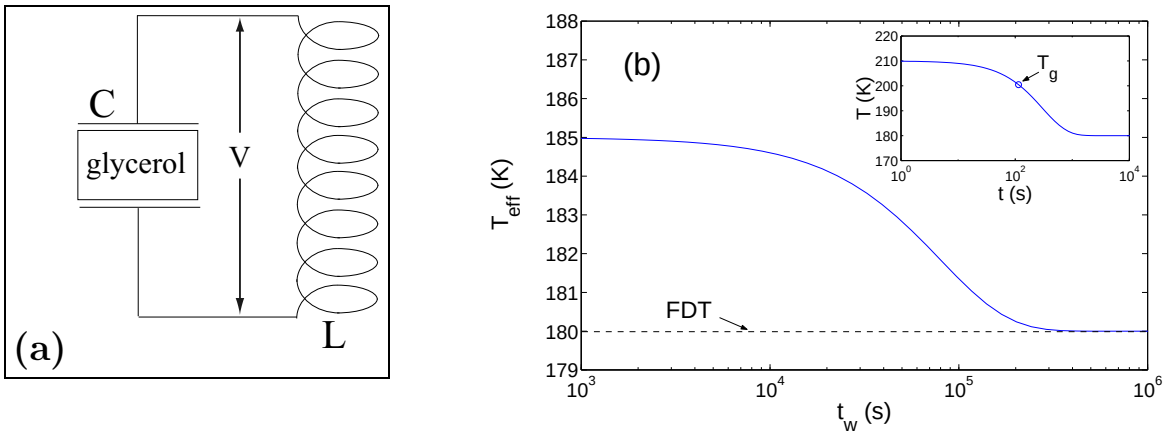

Figure 14: **Experiment on supercooled fluids** (a) Electrical circuit used to measure the FDT violation in Glycerol (b) T_{eff}, measured at 7Hz, versus time, after a quench from $220K$ to $180K$. The sample thermal history is sketched in the inset. See text for more details

from the measure of $< \delta\rho^2 >= C(t_w, t_w)$, and the point $(0, R_o)$ where R_o is the response (isothermal compressibility) measured at large τ and t_w. As it is shown in fig.13 these two points are not enough to determine $T_{eff}(t, t_w)$. In this figure the solid line has slope $1/T$ and corresponds to the FDT. In the figure R_o is certainly smaller then the value predicted by FDT and thus there is a violation. However the curves I and II indicates that several possibilities exist to make the connections between the measured R_o and $C(t_w, t_w)$ measured by the x-ray scattering. For example curves I and II correspond to an infinite T_{eff} and to $T_{eff} \simeq 3T$ respectively.

The main conclusion of this discussion is that the experiment of Wendorff and Fisher [32] is certainly useful to point out that a violation of FDT exists in polymers, but this is not enough to determine T_{eff} and more experiment are needed in order to understand FDR in more details. In the next sections we will describe several experiments whose aim is just that of studying FDR in several materials and with different techniques.

3.2 Supercooled liquid experiment

This experiment has been performed by Grigera and Israeloff [44] by realizing an experiment first proposed in ref.[10]. The idea is in some way that of measuring the temperature an electric harmonic oscillator, composed by a perfect inductance L and a capacitor C whose dielectric is just an aging material. As the dielectric constant is complex then $C = C' + iC"$. In the experiment of ref.[44] the dielectric is just Glycerol which is a liquid with $T_g = 196K$. The schematic diagram of the circuit is drawn in fig.14. The electrical impedance of this circuit is:

$$Z(\omega) = \frac{i\ \omega\ L}{1 - \omega^2\ C'\ L\ + i\omega^2\ C"\ L} \tag{7}$$

The FDR for an electrical impedance $Z(\omega)$ is given by a generalization of the Nyquist

formula:

$$S_V(\omega, t_w) = \frac{2k_B T_{eff}(\omega, t_w)}{\pi}\ Re[Z(\omega, t_w)] \tag{8}$$

where $S_V(\omega, t_w)$ is the spectrum of the voltage thermal fluctuations measured on the impedance. For the circuit of fig.14(a), eq.8 becomes :

$$S_V(\omega, t_w) = \frac{2k_B T_{eff}(\omega, t_w)\omega^3 L^2 C"}{\pi\ [(1-\omega^2\ L\ C')^2 + \omega^4 L^2 C"^2} \tag{9}$$

The idea of this experimental configuration is very smart because from the single measure of $S_V(\omega, t_w)$ one can extract simultaneously the value of T_{eff} and C. Indeed, if L is known, the resonance frequency is $\omega_o = 1/\sqrt{LC'}$, the resonance width is proportional to C" and the amplitude at resonance is proportional to T_{eff}. Except for several experimental details this is the technique used to study FDR in glycerol [44]. In the experiment of ref.[44] the resonance frequency is $7Hz$. The glycerol sample is heated at $210K$ and quenched at $180K$ in about $10^3 s$ (see inset of fig.14(b)). The zero of t_w is taken when the temperature is equal to T_g. The main result of the experiment of ref.[44] is that $T_{eff}(\omega_o, t_w)$ evolves as sketched in fig.14(b). In spite of the fact that, at $t_w = 1000s$ the sample temperature is already at the thermal bath temperature, we see that FDT is violated and the violation lasts for a time which is much larger than $1/\omega_o$. It finally relaxes to $180K$ after $10^5 s$.

The drawback of this interesting experiment is that one has access only to $T_{eff}(\omega_o, t_w)$, that is to the value of the effective temperature at resonance. Therefore there is no idea on how the effective temperature evolves as a function of ω at different t_w. The experiments described in the next sections analyze this problem.

3.3 Gel electric properties

FDR, eq.1, is studied during the colloidal glass formation in Laponite RD [50], a synthetic clay consisting of discoid charged particles. It disperses rapidly in water and solidifies even for very low mass fraction. Physical properties of this preparation evolves for a long time, even after the sol-gel transition, and have shown many similarities with standard glass aging [3, 51]. Recent experiments [51] have proved that the structure function of Laponite at low concentration (less than 3% mass fraction) is close to that of a glass. As in our experiment the Laponite concentration is low, we call the solid like Laponite solution either a colloidal glass or simply a glass.

3.3.1 The experimental apparatus

The Laponite [50] solution is used as a conductive liquid between the two golden coated electrodes of a cell (see fig.1). It is prepared in a clean N_2 atmosphere to avoid CO_2 and O_2 contamination, which perturbs the electrical measurements. Laponite particles are dissolved at a concentration of 2.5% mass fraction in pure water under vigorous stirring during $300s$. To avoid the existence of any initial structure in the sol, we pass the solution through a $1\mu m$ filter when filling our cell. This instant defines the origin of the aging time t_w (the filling

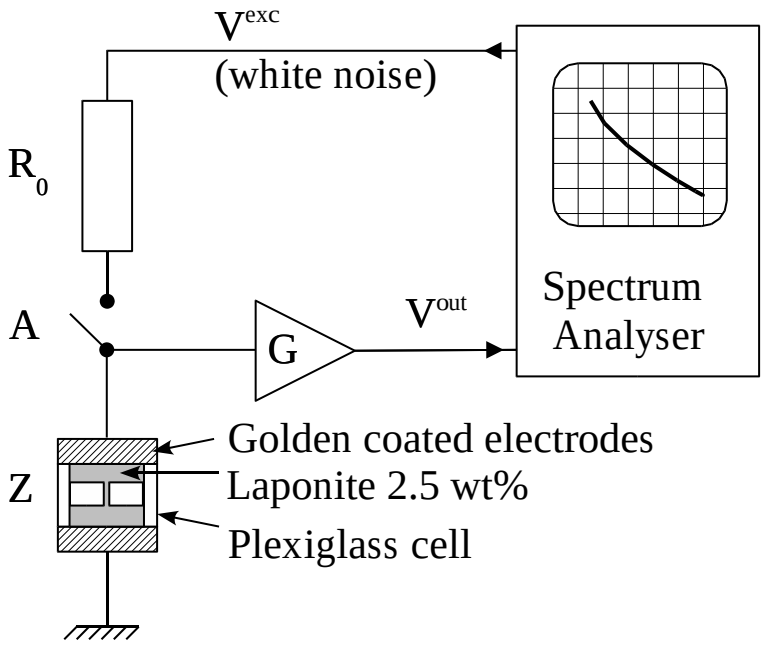

Figure 15: **Laponite experimental set-up** The impedance under test Z is a cell filled with a $2.5wt\%$ Laponite sol. The electrodes of the cell are golden coated to avoid oxidation. One of the two electrodes is grounded whereas the other is connected to the entrance of a low noise voltage amplifier characterized by a voltage amplification G. With a spectrum analyzer, we alternately record the frequency response $FR(\omega) =< V^{out}/V^{exc} >$ (switch A closed) and the spectrum $S(\omega) =< |V^{out}|^2 >$ (switch A opened). The input voltage V^{exc} is a white noise excitation, thus from $FR(\omega)$ we derive the impedance $Z(\omega)$ as a function of ω, that is $Z(\omega) = R_0/(G/FR(\omega) - 1)$; whereas from $S(\omega)$, we can estimate the voltage noise of Z, specifically $S_Z(\omega) = [S(\omega) - S_a(\omega)]/G^2$ where $S_a(\omega)$ is the noise spectral density of the amplifier

of the cell takes roughly two minutes, which can be considered the maximum inaccuracy of t_w). The sample is then sealed so that no pollution or evaporation of the solvent can occur. At this concentration, the light scattering experiments show that Laponite [50] structure functions are still evolving $500h$ after the preparation [3]. We only study the beginning of this glass formation process.

The two electrodes of the cell are connected to our measurement system, where we alternately record the cell electrical impedance $Z(t_w, \omega)$ and the voltage noise density $S_Z(t_w, \omega)$ (see fig.15). Taking into account that in this configuration $Im\left[\chi_{Vq}(t_w, \omega)\right] = \omega Re\left[Z(t_w, \omega)\right]$, one obtains from eq.2 that the effective temperature of the Laponite solution as a function of the aging time and frequency is:

$$T_{eff}(t_w, \omega) = \pi S_Z(t_w, \omega)/2k_B Re\left[Z(t_w, \omega)\right] \tag{10}$$

which, as already mentioned in sec.3.2 (eq.8) is an extension of the Nyquist formula.

The electrical impedance of the sample is the sum of 2 effects: the bulk is purely con-

ductive, the ions of the solution follow the forcing field, whereas the interfaces between the solution and the electrodes give mainly a capacitive effect due to the presence of the Debye layer [52]. This beahvior has been validated using a four-electrode potentiostatic technique [53] to make sure that the capacitive effect is only due to the surface. In order to test only bulk properties, the geometry of the cell is tuned to push the surface contribution to low frequencies. Specifically the cell is composed by two large reservoirs in contact with the electrodes which have an area of $25cm^2$. The reservoirs are connected by a rigid tube (see fig.15) whose section and length give the main contribution to the bulk electrical resistance. Thus by changing the sizes of the tube the bulk resistance can be changed from 300Ω to $100K\Omega$. We checked that the dynamics of the system does not depend on the value of the bulk resistance. For a bulk resistance of about $10^5\Omega$ the cutoff frequency of the equivalent R-C circuit (composed by the series of the Debye layers plus the bulk resistance) is about $0.02Hz$. In other words above this frequency the imaginary part of the cell impedance is about zero.

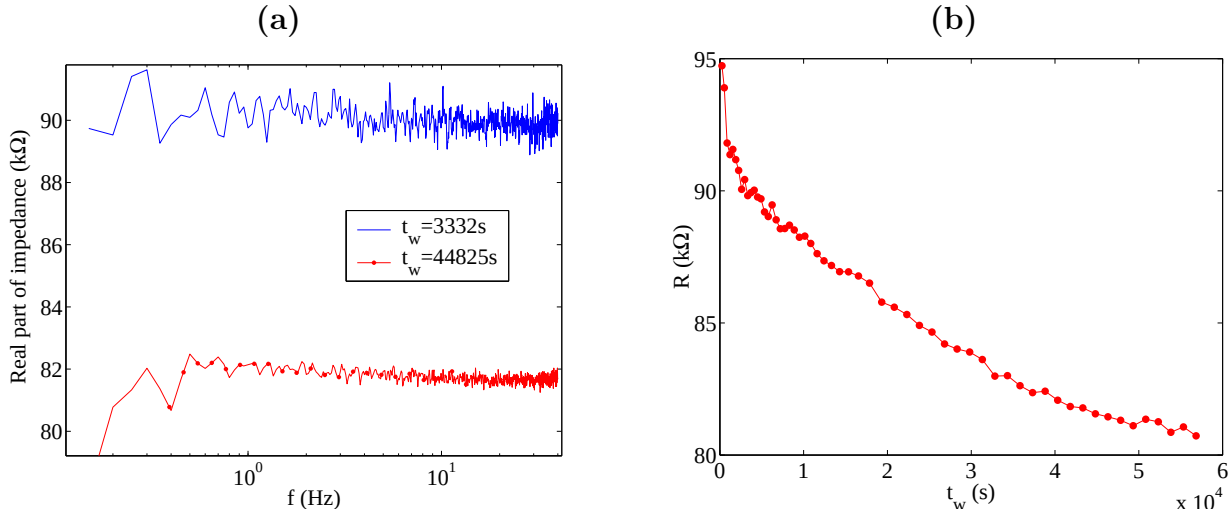

Figure 16: **Laponite response function** (a) Frequency dependence of a sample impedance for 2 different aging times: continuous line $t_w = 3332s$; $(\bullet)t_w = 44825s$.(b) Time evolution of the resistance. This long time evolution is the signature of the aging of the sol. In spite of the decreasing mobility of Laponite particles in solution during the gelation, the electrical conductivity increases.

3.3.2 FDR measurements

In fig.16(a), we plot the real part of the impedance as a function of the frequency f, for a typical experiment and two different times. The time evolution of the resistance of one of our sample is plotted in fig.16(b): it is still decaying in a non trivial way after $24h$, showing that the sample has not reached any equilibrium yet. This aging is consistent with that observed in light scattering experiments [3].

As the dissipative part of the impedance $Re(Z)$ is weakly time and frequency dependent,

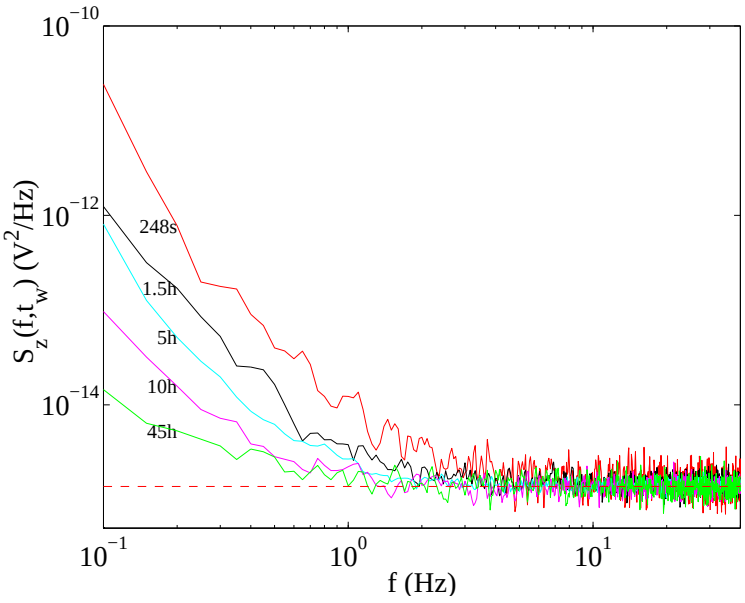

Figure 17: **Voltage fluctuations for Laponite** Voltage noise density of one sample for different aging times. The horizontal dashed line is the FDT prediction

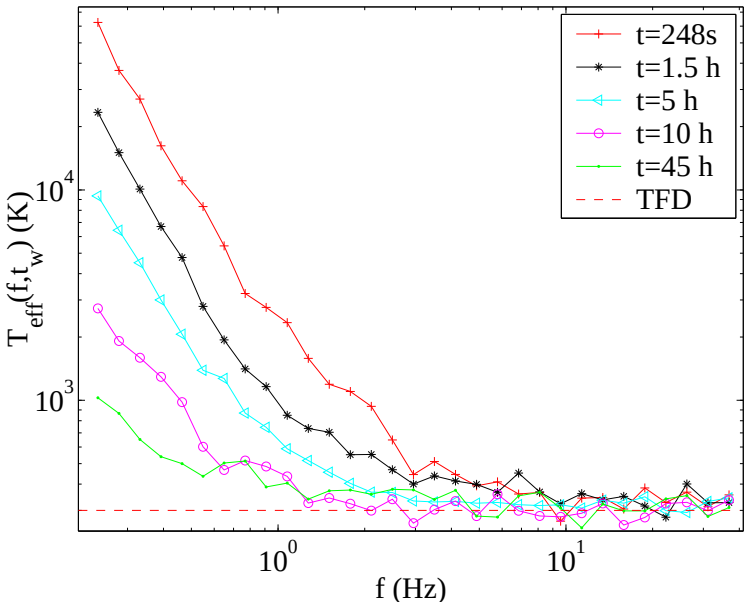

Figure 18: **Effective temperature of Laponite**. Effective temperature as a function of frequency for different aging times. As S_Z in fig.17, T_{eff} strongly increases and reaches huge values for low frequencies and short aging times.

one would expect from the Nyquist formula that so does the voltage noise density S_Z. But as shown in fig.17, FDT must be strongly violated for the lowest frequencies and earliest times of our experiment: S_Z changes by several orders of magnitude between highest values

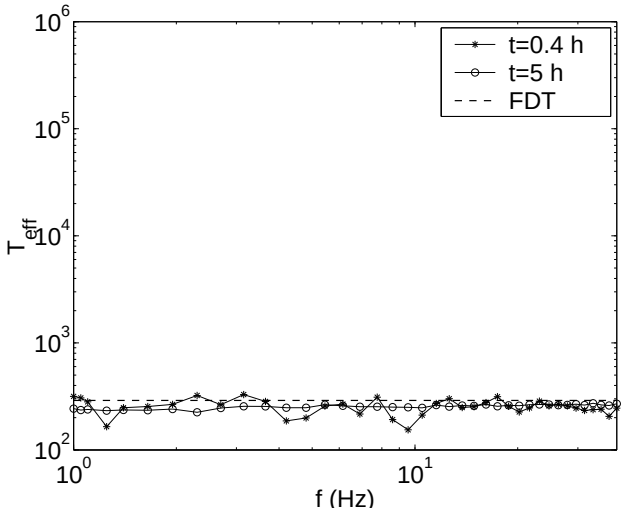

Figure 19: **Effective temperature of an $NaOH$ solution in water**. The effective temperature is plotted as a function of frequency for two different times after the preparation. This solution has a pH close to that of the Laponite, and no violation is observed in this case for any aging time.

and the high frequency tail [1]. This violation is clearly illustrated by the behavior of the effective temperature in fig.18 [2]. For long times and high frequencies, the FDT holds and the measured temperature is the room one ($300K$); whereas for early times T_{eff} climbs up to $3.10^3 K$ at $1Hz$. Moreover, T_{eff} could be even larger for lower frequencies and lower aging times: indeed, we found in all the tested samples no evidence of a saturation of this effective temperature in our measurement range. In order to be sure that the observed violation is not due to an artifact of the experimental procedure, we filled the cell with an electrolyte solution with pH close to that of the Laponite sol such that the electrical impedance of the cell was the same. Specifically we filled the cell with $NaOH$ solution in water at a concentration of 10^{-3} $mol.l^{-1}$. The results of the measurements of T_{eff} are shown in fig.19 at two different times after the sample preparation. In this case we did not observe any violation of FDT at any time.

3.3.3 Statistical analysis of the noise

In order to understand such a behavior we have directly analyzed the noise voltage across the Laponite cell. This test can be safely done in our experimental apparatus because the amplifier noise is negligible with respect to the thermal noise of the Laponite cell even when FDT is satisfied. In fig.20(a) we plot a typical signal measured $2h$ after the gel preparation

[1] This low frequency noise cannot be confused with the standard $1/f$ noise observed in many electronic devices. We recall that the $1/f$ appears only when an external current produced by an external potential goes through the device. In our cell no external potential is applied.

[2] The usual representation of the effective temperature in simulations is the slope of the response versus correlation plot, but it is not suited for our experimental data: the system being almost only dissipative, the response function is close to a delta distribution, thus FDT is only one point in this representation.

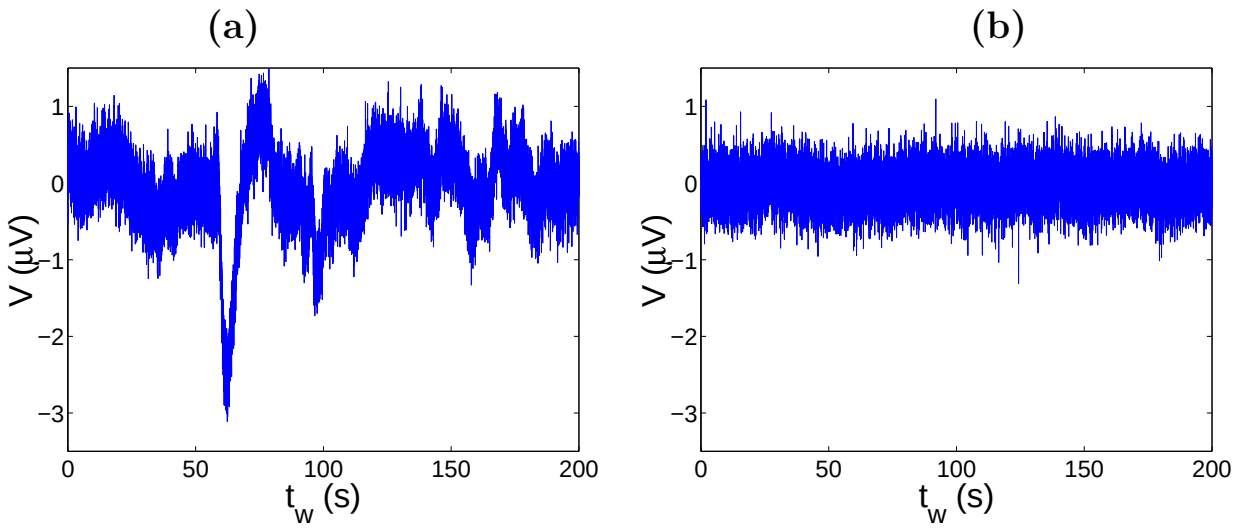

Figure 20: **Voltage noise signal in Laponite** . (a) Noise signal, 2 hours after the Laponite preparation, when FDT is violated. (b) Typical noise signal when FDT is not violated.

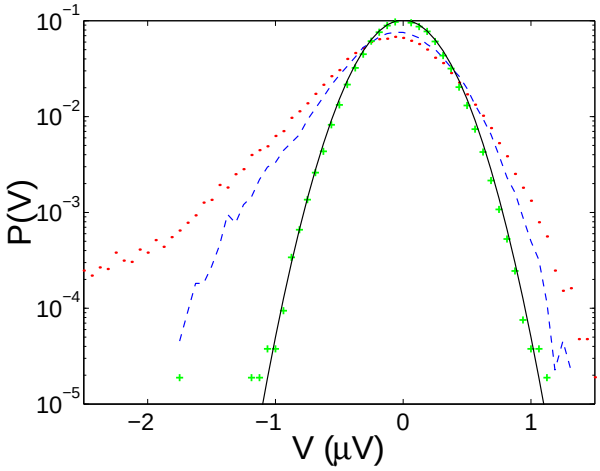

Figure 21: **PDF of the voltage noise in Laponite** . Typical PDF of the noise signal at different times after preparation, with from top to bottom: $(...)t_w = 1h$, $(--)t_w = 2h$, $(+)t_w = 50h$. The continuous line is obtained from the FDT prediction.

when the FDT is strongly violated. The signal plotted in fig.20(b) has been measured when the system is relaxed and FDT is satisfied in all the frequency range. By comparing the two signals we immediately realize that there are very important differences. The signal in fig.20(a) is interrupted by bursts of very large amplitude which are responsible for the increasing of the noise in the low frequency spectra (see fig.17). The relaxation time of the bursts has no particular meaning, because it corresponds just to the characteristic time of the filter used to eliminate the very low frequency trends. As time goes on, the amplitude of the bursts reduces and the time between two consecutive bursts becomes longer and longer.

Finally they disappear as can be seen in the signal of fig.20(b) recorded after $50h$ when the system satisfies FDT. The evolution of the intermittent properties of the noise can be characterized by studying the probability density function (PDF) of the signal as a function of time. To compute the PDF, the time series are divided in several time windows and the PDF are computed in each of these windows. Afterwards the results of several experiments are averaged. The PDF computed at different times are plotted in fig.21. We see that at short t_w the PDF presents very high tails which slowly disappear at longer t_w. Finally a Gaussian shape is recovered at $t_w = 16h$. This kind of evolution of the PDF clearly indicates that the signal is very intermittent at the very beginning and it relaxes to the Gaussian noise at very long times.

The comparison of these results with aging models will be done in the conclusions. We prefer to describe now another experiment in a completely different material.

3.4 Polycarbonate dielectric properties

In order to give more insight into the problem of the violation of FDT and of the intermittent beahvior discussed in the previous section we have done wide band ($20mHz - 100Hz$) measurements of the dielectric susceptibility and of the polarization noise in a polymer glass: polycarbonate. We present in this lecture several results which show a strong violation of the FDT when this material is quenched from the molten state to below its glass-transition temperature. The effective temperature defined by eq.2 slowly relaxes towards the bath temperature. The violation is observed even at $\omega t_w \gg 1$ and it may last for more than $3h$ for $f > 1Hz$.

3.4.1 The experimental apparatus

The polymer used in this investigation is Makrofol DE 1-1 C, a bisphenol A polycarbonate, with $T_g \simeq 419K$, produced by Bayer in form of foils. We have chosen this material because it has a wide temperature range of strong aging [1]. This polymer is totally amorphous: there is no evidence of crystallinity [54]. Nevertheless, the internal structure of polycarbonate changes and relaxes as a result of a change in the chain conformation by molecular motions [1],[55],[56]. Many studies of the dielectric susceptibility of this material exist, but no one had an interest on the problem of noise measurements.

In our experiment polycarbonate is used as the dielectric of a capacitor. The capacitor is composed by 14 cylindrical capacitors in parallel in order to reduce the resistance of the sample and to increase its capacity. Each capacitor is made of two aluminum electrodes, $12\mu m$ thick, and by a disk of polycarbonate of diameter $12cm$ and thickness $125\mu m$. The experimental set-up is shown in fig.22(a). The 14 capacitors are sandwiched together and put inside two thick aluminum plates which contain an air circulation used to regulate the sample temperature. This mechanical design of the capacitor is very stable and gives very reproducible results even after many temperature quenches. The capacitor is inside two Faraday screens to insulate it from external noise. The temperature of the sample is controlled within a few percent. Fast quench of about $50K/min$ are obtained by injecting Nitrogen vapor in the air circulation of the aluminum plates. The electrical impedance of the capacitor is $Z(\omega, t_w) = R/(1 + i\omega\ R\ C)$, where C is the capacitance and R is a parallel

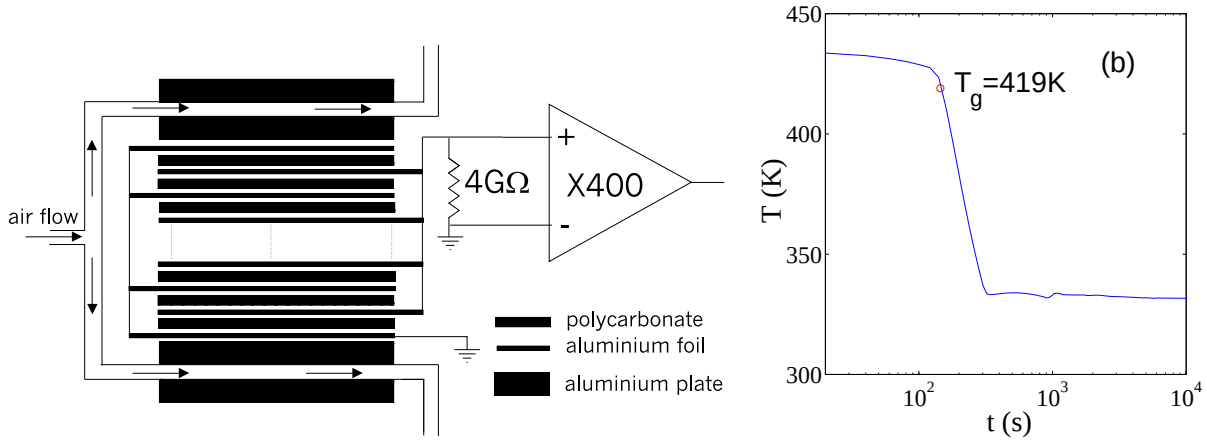

Figure 22: (a) **Polycarbonate experimental set-up** (b) **Typical temperature quench:** from $T_i = 433K$ to $T_f = 333K$, the origin of t_w is at $T = T_g$.

resistance which accounts for the complex dielectric susceptibility. It is measured using a Novocontrol Dielectric Analyzer. The noise spectrum of this impedance $S_Z(\omega, t_w)$ is:

$$S_Z(f, t_w) = 4\ k_B\ T_{eff}(f, t_w)\ Re[Z(\omega, t_w)] = \frac{4\ k_B\ T_{eff}(f, t_w)\ R}{1 + (\omega\ R\ C)^2} \tag{11}$$

where T_{eff} is the effective temperature of the sample. In order to measure $S_Z(f, t_w)$, we have made a differential amplifier based on selected low noise JFET(2N6453 InterFET Corporation), whose input has been polarized by a resistance $R_i = 4G\Omega$. Above $2Hz$, the input voltage noise of this amplifier is $5nV/\sqrt{Hz}$ and the input current noise is about $1fA/\sqrt{Hz}$. The output signal of the amplifier is analyzed either by an HP3562A dynamic signal analyzer or directly acquired by a NI4462 card. It is easy to show that the measured spectrum at the amplifier input is:

$$S_V(f, t_w) \quad = \quad \frac{4\ k_B\ R\ R_i\ \ (\ T_{eff}(f, t_w)\ R_i + \ T_R\ R + S_\xi(f)\ R\ R_i)}{(R + R_i)^2 + (\omega\ R\ R_i\ C)^2} + S_\eta(f) \tag{12}$$

where T_R is the temperature of R_i and S_η and S_ξ are respectively the voltage and the current noise spectrum of the amplifier. In order to reach the desired statistical accuracy of $S_V(f, t_w)$, we averaged the results of many experiments. In each of these experiments the sample is first heated to $T_i = 433K$. It is maintained at this temperature for 4 hours in order to reinitialize its thermal history. Then it is quenched from T_i to $T_f = 333K$ in about 2 minutes. A typical thermal history of the quench is shown in fig.22(b). The reproducibility of the capacitor impedance, during this thermal cycle is always better than 1%. The origin of aging time t_w is the instant when the capacitor temperature is at $T_g \simeq 419K$, which of course may depend on the cooling rate. However adjustment of T_g of a few degrees will shift the time axis by at most $30s$, without affecting our results.

3.4.2 FDR measurements

In fig.23(a) and (b), we plot the measured values of R and C as a function of f at T_i and at T_f for $t_w \geqslant 200s$. We see that lowering temperature R increases and C decreases. At T_f aging is small and extremely slow. Thus for $t_w > 200s$ the impedance can be considered constant without affecting our results. From the data plotted in fig.23 (a) and (b) one finds that $R = 10^{10}(1 \pm 0.05)\ f^{-1.05\pm0.01}\ \Omega$ and $C = (21.5 \pm 0.05)nF$. In fig.23(a) we also plot the total resistance at the amplifier input which is the parallel of the capacitor impedance with R_i. We see that at T_f the input impedance of the amplifier is negligible for $f > 10Hz$, whereas it has to be taken into account at slower frequencies.

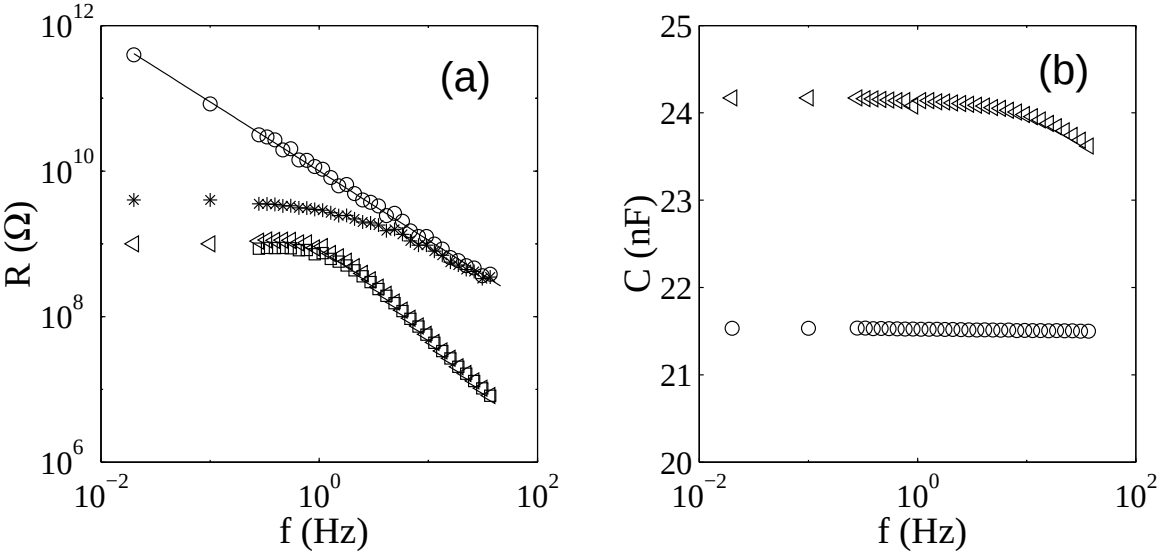

Figure 23: **Polycarbonate response function** (a) Polycarbonate resistance R as a function of frequency measured at $T_i = 433K$ ($\triangleleft$) and at $T_f = 333k$ ($\circ$). The effect of the $4G\Omega$ input resistance is also shown at $T = 433K$ ($\square$) and at $T = 333K$ ($*$). (b) Polycarbonate capacitance versus frequency measured at $T_i = 433K$ ($\triangleleft$) and at $T_f = 333k$ ($\circ$).

Fig.24(a) represents the evolution of $S_V(f, t_w)$ after a quench. Each spectrum is obtained as an average in a time window starting at t_w. The time window increases with t_w so to reduce error for large t_w. Then the results of 7 quenches have been averaged. At the longest time ($t_w = 1\ day$) the equilibrium FDT prediction (continuous line) is quite well satisfied. We clearly see that FDT is strongly violated for all frequencies at short times. Then high frequencies relax on the FDT, but there is a persistence of the violation for lower frequencies. The amount of the violation can be estimated by the best fit of $T_{eff}(f, t_w)$ in eq.12 where all other parameters are known. We started at very large t_w when the system is relaxed and $T_{eff} = T$ for all frequencies. Inserting the values in eq.12 and using the S_V measured at $t_w = 1day$ we find $T_{eff} \simeq 333K$, within error bars for all frequencies (see fig.24b). At short t_w data show that $T_{eff}(f, t_w) \simeq T_f$ for f larger than a cutoff frequency $f_o(t_w)$ which is a function of t_w. In contrast, for $f < f_o(t_w)$ we find that T_{eff} is: $T_{eff}(f, t_w) \propto f^{-A(t_w)}$, with $A(t_w) \simeq 1$. This frequency dependence of $T_{eff}(f, t_w)$ is quite well approximated by

$$T_{eff}(f,t_w) = T_f\ [\ 1\ +\ (\frac{f}{f_o(t_w)})^{-A(t_w)}\ ] \tag{13}$$

where $A(t_w)$ and $f_o(t_w)$ are the fitting parameters. We find that $1 < A(t_w) < 1.2$ for all the data set. Furthermore for $t_w \geq 250$, it is enough to keep $A(t_w) = 1.2$ to fit the data within error bars. For $t_w < 250s$ we fixed $A(t) = 1$. Thus the only free parameter in eq.13 is $f_o(t_w)$. The continuous lines in fig.24(a) are the best fits of S_V found inserting eq.13 in eq.12.

In fig.24(b) we plot the estimated $T_{eff}(f,t_w)$ as a function of frequency at different t_w. We see that just after the quench $T_{eff}(f,t_w)$ is much larger than T_f in all the frequency interval. High frequencies rapidly decay towards the FDT prediction whereas at the smallest frequencies $T_{eff} \simeq 10^5 K$. Moreover we notice that low frequencies decay more slowly than high frequencies and that the evolution of $T_{eff}(f,t_w)$ towards the equilibrium value is very slow. From the data of fig.24(b) and eq.13, it is easy to see that $T_{eff}(f,t_w)$ can be superposed onto a master curve by plotting them as a function of $f/f_o(t_w)$. The function $f_o(t_w)$ is a decreasing function of t_w, but the dependence is not a simple one, as it can be seen in the inset of fig.24(b). The continuous straight line is not fit, it represents $f_o(t_w) \propto 1/t_w$ which seems a reasonable approximation for these data. For $t_w > 10^4 s$ we find the $f_o < 1Hz$. Thus we cannot follow the evolution of T_{eff} anymore because the contribution of the experimental noise on S_V is too big, as it is shown in fig.24(b) by the increasing of the error bars for $t_w = 1\ day$ and $f < 0.1Hz$.

Before discussing these experimental results we want to compare them to the single frequency experiment performed on glycerol (sec.3.2) [44]. In this experiment, T_{eff} has been measured only at $7Hz$. Thus we studied how $T_{eff}(7Hz,t_w)$ depends on t_w at $7Hz$ in our experiment. The time evolution of $T_{eff}(7Hz,t_w)$ is plotted as a function of t_w in fig.25a). The time evolution of $T_{eff}(2Hz,t_w)$ is also plotted just to show the large temperature difference between two frequencies. Let us consider the evolution at $7Hz$ only. As in the experiment described in sec.3.2 ref.[44], we confirm the fact that the violation is observed even if $\omega t_w >> 1$, which is in contrast with theoretical predictions. The biggest violation is for short times after the quench where the effective temperature is surprisingly huge: around 800K at $7Hz$ and $t_w = 300s$. In the experiment on glycerol the first data reported are for $t_w > 1000s$. Thus if we consider only data at $t_w > 1000s$ in fig.25a) we see that our results are close to those of ref.[44]. Indeed at $t_w = 1000s$ we find in our experiment $(T_{eff} - T_f)/(T_g - T_f) \simeq 2.4$. The glycerol data give $(T_{eff} - T_f)/(T_g - T_f) \simeq 1$. Thus the relative violations of FDT at $7Hz$ are very close in glycerol and polycarbonate. However it would be interesting to check whether at shorter times and at lower frequencies large T_{eff} could be observed in glycerol too.

In order to compare with theoretical predictions [30, 10] and recent spin glass experiment [47] we may plot the integrated response $R(t,t_w)$ as a function of the correlation $C(t,t_w)$. The latter is obtained inserting measured $T_{eff}(f,t_w)$ in eq.11 and by Fourier transforming this equation. $R(t,t_w)$ can be computed by Fourier transforming $Real[Z(\omega,t_w)]$. FDR now takes the form [10, 11]:

$$-C(t,t_w) + C(t_w,t_w) = k_B\ T_{eff}(t,t_w)\ R(t,t_w) \tag{14}$$

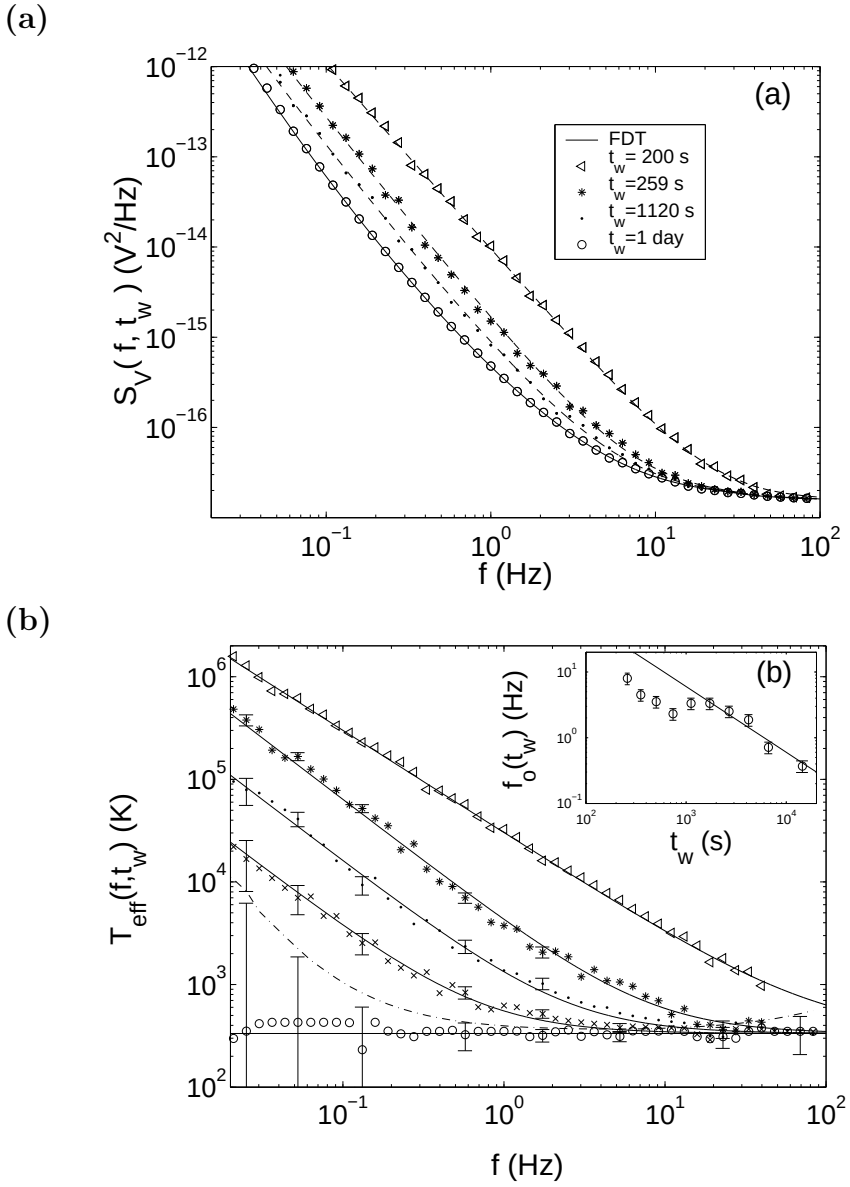

Figure 24: **Voltage noise and effective temperature in polycarbonate.** (a) Noise power spectral density $S_V(f, t_w)$ measured at $T_f = 333K$ and different t_w. The spectra are the average over seven quenches. The continuous line is the FDT prediction. Dashed lines are the fit obtained using eq.12 and eq.13 (see text for details). (b) Effective temperature vs frequency at $T_f = 333K$ for different aging times: ($\lhd$) $tw = 200\ s$, ($*$) $tw = 260s$, $\bullet$ $tw = 2580s$, ($\times$)$t_w = 6542s$, ($\circ$)$t_w = 1\ day$. The continuous lines are the fits obtained using eq.13. The horizontal straight line is the FDT prediction. The dot dashed line corresponds to the limit where the FDT violation can be detected. In the inset the frequency $f_o(t_w)$, defined in eq.13, is plotted as a function of t_w. The continuous line is not a fit, but it corresponds to $f_o(t_w) \propto 1/t_w$.

In the inset of fig.25(b), we see that for $t_w > 300s$ the shape of the decay of $C(t_w, t)$ remains

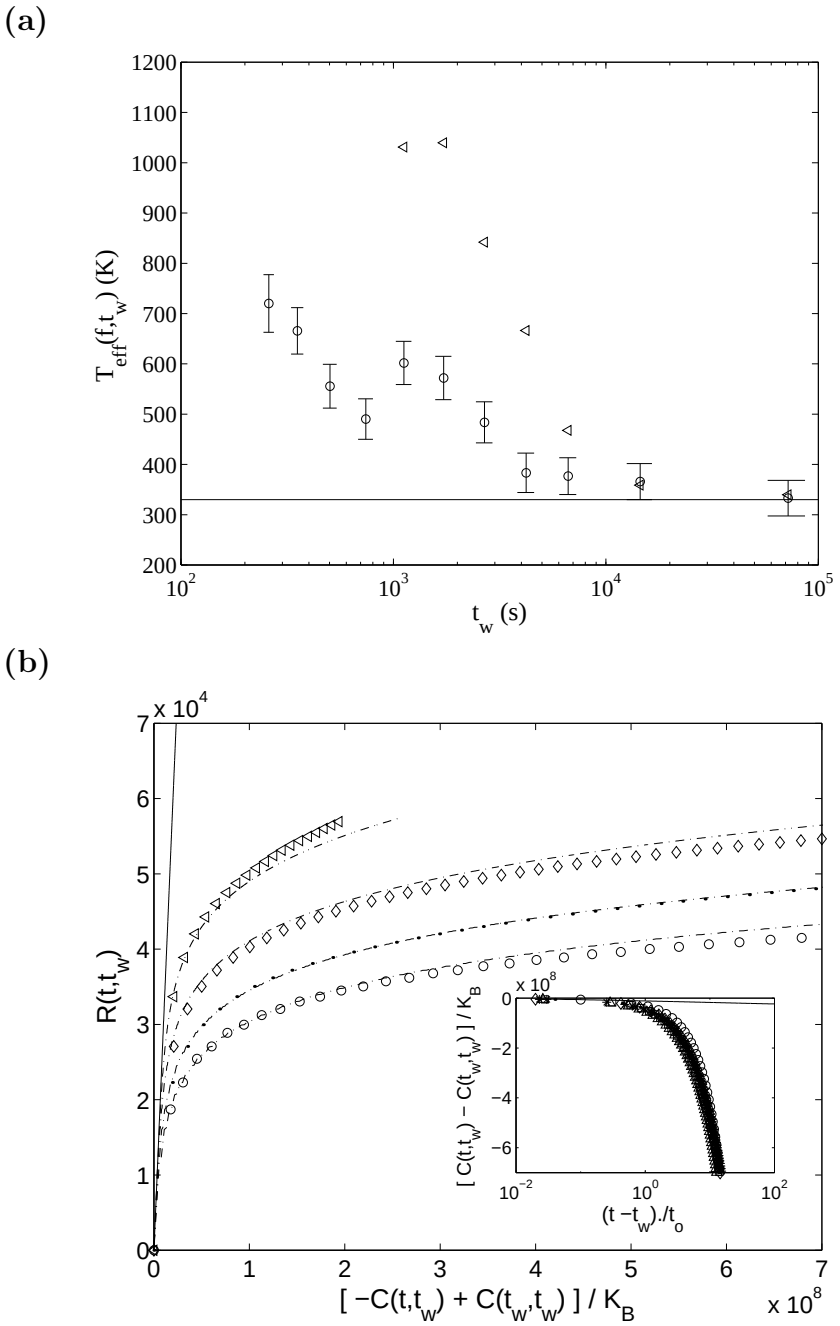

Figure 25: **Violation of FDT in polycarbonate.** (a) Effective temperature at $7Hz$ ($\circ$) and $2Hz$ ($\lhd$) measured as a function of t_w at $T_f = 333K$. b) Plot of the integrated response $R(t, t_w)$ as a function of $-C(t, t_w) + C(t_w, t_w)$ at different t_w. Symbols correspond to the data: ($\circ$) $tw = 256s$, ($\bullet$)$t_w = 353s$, ($\Diamond$)$t_w = 4200s$, ($\lhd$)$t_w = 6542s$. The dashed lines are obtained from the best fits (see text for details). The continuous straight line is the FDT prediction. In the inset $C(t, t_w) - C(t_w, t_w)$ is plotted as a function of time for several $tw = 250s; 353s; 503s; 1120s; 1624s; 2583s; 4200s$. The correlation functions have been superposed by scaling $t - t_w$ by a characteristic time $t_o(t_w)$ which is an increasing function of t_w.

essentially the same. Indeed data for different t_w can be scaled onto a single master curve by plotting $C(t_w, t)$ as a function $(t - t_w)/t_o(t_w)$, where $t_o(t_w)$ is an increasing function of t_w: approximately $t_o(t_w) \propto log(t_w)$ for $t_w > 500s$. The self-similarity of correlation functions, found on our dielectric data, is a characteristic of the universal picture of aging [9, 10, 36, 37, 57], which has been also observed in spin-glass experiment [47] and in the structure function of the dynamic light scattering of colloidal gels [58]. Thus our results confirm that this picture of aging applies also to the polymer dielectric measurements. To further investigate this aging, we plot, in fig.25b), $R(t, t_w)$ as a function $(-C(t, t_w) + C(t_w, t_w))/k_B$ at different t_w. The slope of this graph gives $1/T_{eff}$. The symbols correspond to the data whereas the dashed line are obtained by inserting the best fit of T_{eff} in eq.13, in eq.11. We clearly see that data at small $C(t, t_w)$ asymptotically converge to an horizontal straight line, which means that the system has an infinite temperature. At short time, large $C(t, t_w)$, FDT prediction is recovered (continuous straight line of slope $1/T_f$). This result is quite different to what has been observed in recent experiments on spin glasses where $T_{eff} \simeq 5T_g$ has been measured [47]. In contrast infinite T_{eff} has been observed during the sol gel transition [45] and in numerical simulation of domain growth phenomena [38].

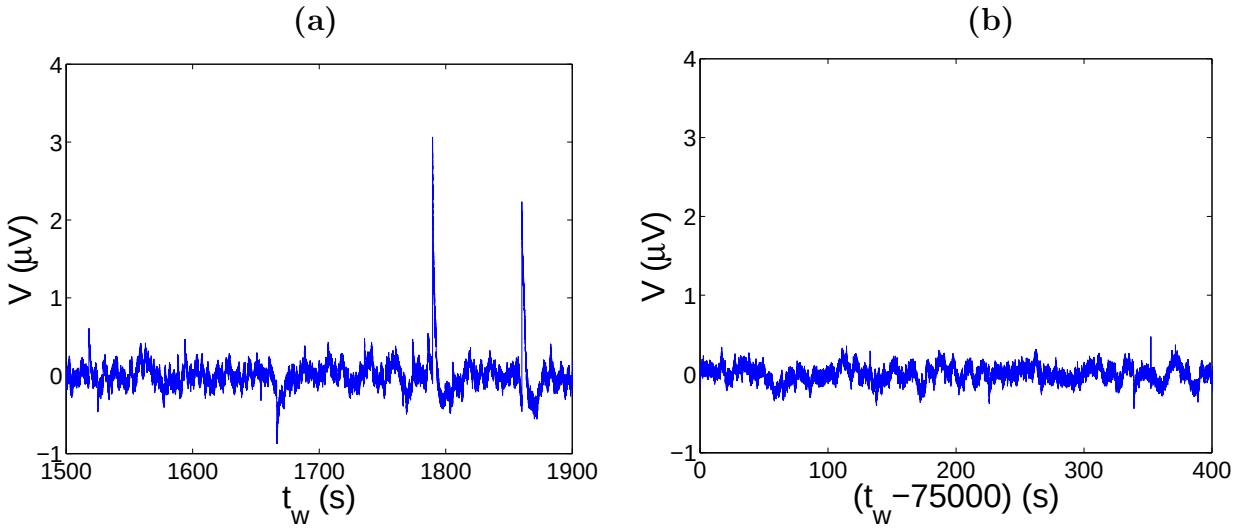

Figure 26: **Voltage noise signal in polycarbonate** Typical noise signal of polycarbonate measured at $1500s < t_w < 1900s$ (a) and $t_w > 75000s$ (b).

3.4.3 Statistical analysis of the noise in Polycarbonate

In order to understand the origin of such large deviations in our experiment we have analyzed the noise signal. We find that the signal is characterized by large intermittent events which produce low frequency spectra proportional to $f^{-\alpha}$ with $\alpha \simeq 2$. Two typical signals recorded at $1500s < t_w < 1900s$ and $t_w > 75000s$ are plotted in fig.26. We clearly see that in the signal recorded at $1500s < t_w < 1900s$ there are very large bursts which are on the origin of the frequency spectra discussed in the previous section. In contrast in the signal (fig.26b), which was recorded at $t_w > 75000s$ when FDT is not violated, the bursts are totally disappeared.

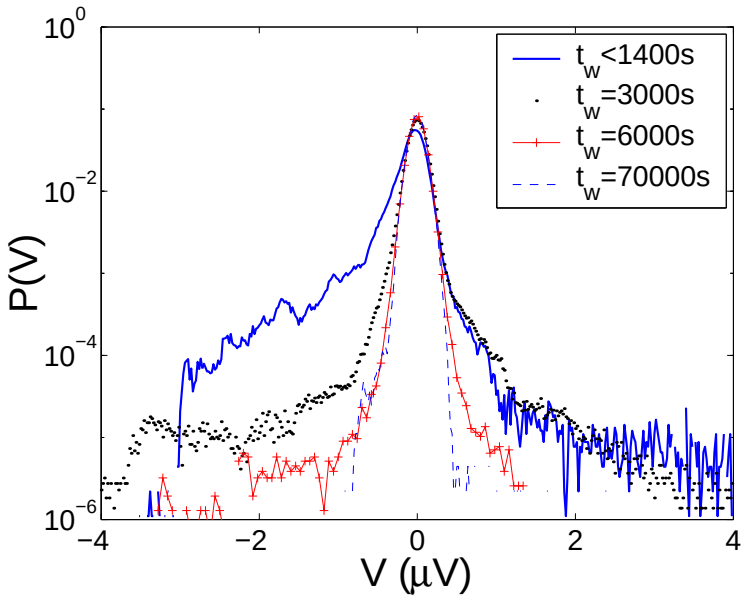

Figure 27: **PDF of voltage noise in polycarbonate** Typical PDF of the noise signal of polycarbonate measured at various t_w

As for Laponite we have studied the PDF of the signal as a function of t_w for polycarbonate. The results are shown in fig.27. We clearly see that the PDF, measured at small t_w, has very high tails which becomes smaller and smaller at large t_w. Finally the Gaussian profile is recovered after $24h$. This strongly intermittent dynamics is reminiscent of the intermittence observed in the local measurements of polymer dielectric properties [59] and in the slow relaxation dynamics of a colloidal gel [60].

3.5 Rheological Measurements

In the previous section we have shown that the FDR is strongly violated by the electrical properties of Laponite. We want to understand whether a violation can be observed in the measurements of other physical properties. Of course there are no reasons to assume that T_{eff} is the same for all the variables [42, 43] but the differences and the analogies found in the evolution of T_{eff} obtained by the measurements of several variables may give new insight on aging theories and on the coupling of the different variables in an aging material. Therefore we performed rheological measurements on Laponite and we checked FDR in these measurements.

3.5.1 Experimental apparatus

To achieve this result we built a new rheometer which is sensitive to thermal fluctuations. The principle of the rheological measurement is a standard one and is illustrated in fig.28. We describe here only the main features, more details can be found in ref.[62, 63]. A rotor of diameter 12mm is inserted in a cylindrical cell. The gap of 1mm between the rotor surface and the cell is filled with the fluid under study. The rotor is suspended by two

steel wires. On the top of the rotor we fixed an optical prism. This prism is part of a Nomarski interferometer [64] which is used to measure the rotation angle θ of the rotor. The sensitivity of this system is better than $10^{-10} rad/\sqrt{Hz}$ corresponding to a torque on the rotor of about $10^{-13} N \cdot m/\sqrt{Hz}$. An external torque Γ_{ext} can be applied to the rotor by using the electrostatic interaction of a capacitor (see fig.28). One of the two electrodes of the capacitor is fixed on the rotor whereas the other is fixed on the cell walls. When a voltage difference V_c is applied on this capacitor the attractive force between these two electrodes produces a torque on the rotor which is equilibrated by the stiffness of the steel wires.

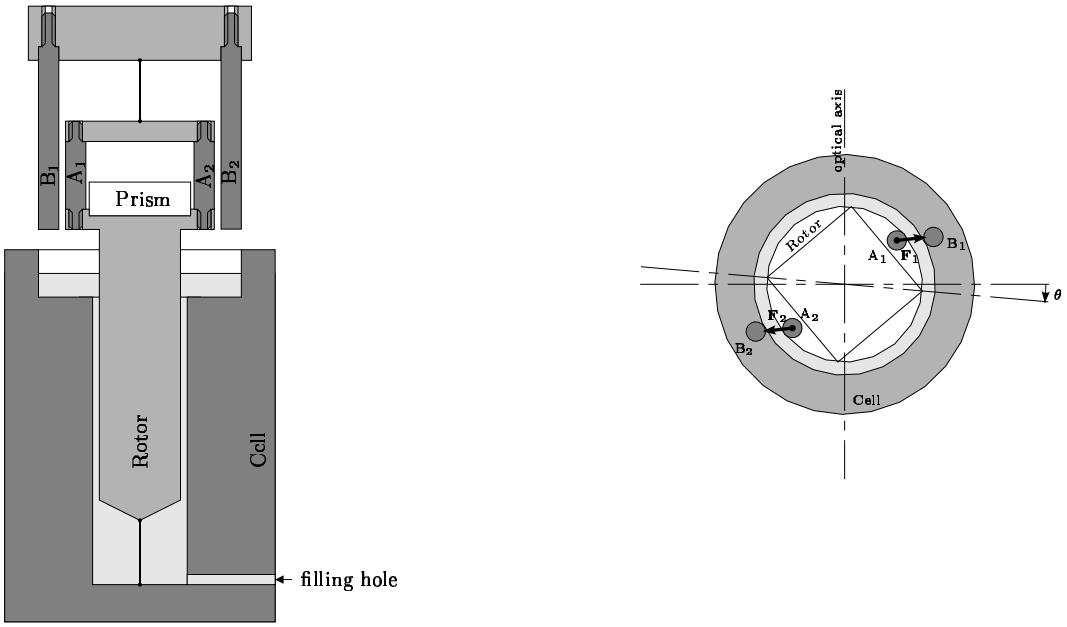

a) **b)**

Figure 28: **Rheometer** Vertical (a) and horizontal (b) cross section of the rheometer. The torque is applied through the electrostatic interaction of electrodes $A_{1,2}$ and $B_{1,2}$ when the voltage V_c is applied to this capacitor.

Let us consider the simple case of a Newtonian fluid of viscosity η. The response of this torsion pendulum in Fourier space is

$$\chi_{\theta\Gamma_{ext}} = \frac{\delta\theta}{\Gamma_{ext}} = \frac{1}{(k - J\omega^2) - i\alpha\eta\omega} \tag{15}$$

where J is the rotor inertia moment, k the steel wires stiffness and α is a geometric factor.

In the experiment we have access to two quantities : the angular position θ of the rotor, and the voltage V_c driving the torque. Γ_{ext} being quadratic in V_c, we add a constant offset to it in order to linearise this relation. For small displacements, the response function $\chi_{\theta\Gamma_{ext}}$ is then simply proportional to $\chi_{\theta V_c}$. The missing constant can be found by performing a inertial calibration of the response: the real part of $1/\chi_{\theta\Gamma_{ext}}$ is a parabola whose quadratic

coefficient is the rotor inertia moment J. J is known with a good precision, and thus can be used to calibrate the measurement.

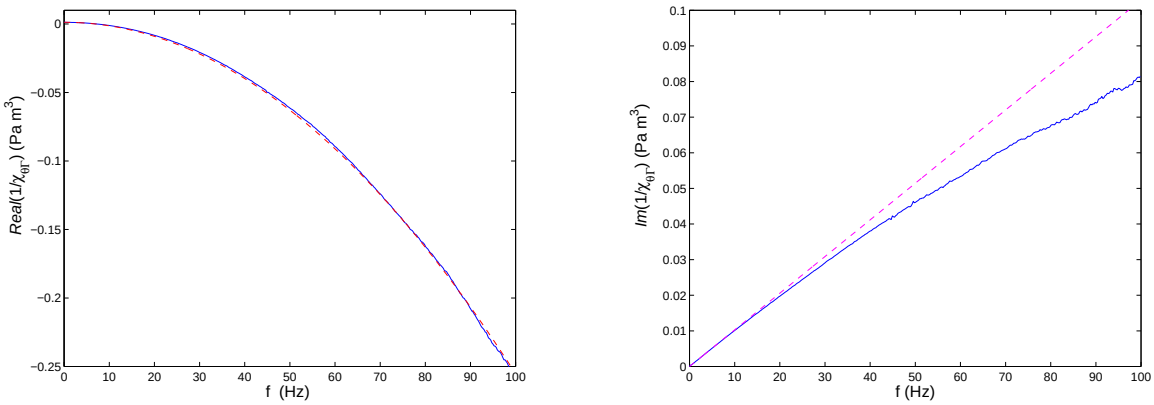

Figure 29: **Response of the rheometer to a white noise excitation.** The real (a) and imaginary (b) part of $1/\chi_{\theta\Gamma_{ext}}$ are plotted as a function of frequency. The rheometer is filled with a viscous oil with $\eta = 2Pa\ s$. The dashed curve in (a) corresponds to a quadratic fit of the data, and allows inertial calibration of the measurement (see text for details). The dashed line in (b) is a linear fit of low frequency data, it is consistent with a newtonian behaviour of the fluid.

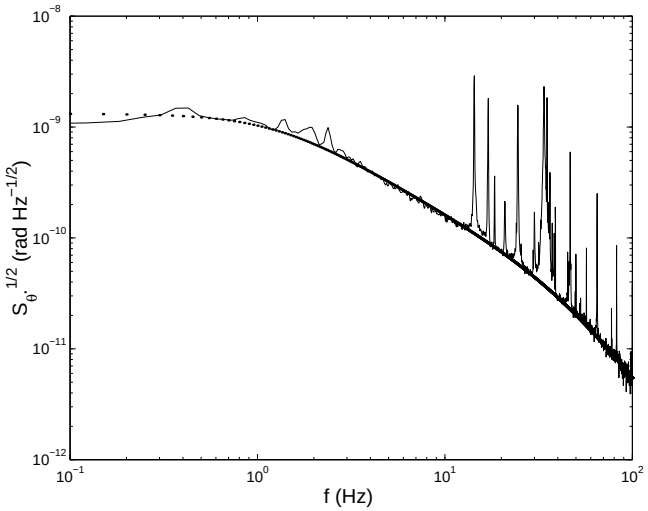

Figure 30: **Spectrum of the thermal fluctuations of θ.** The rheometer is filled with the same oil used to measure the response reported in fig.29. The continuous line is the result of the measurement whereas the dashed line is computed inserting in eq.16 the measured response of the rheometer and $T = 300K$.

This rheometer has been tested using a silicon oil with $\eta = 2Pa\ s$. We first measure the

response by using a white noise voltage exitation for V_c with an amplitude corresponding to a torque $\Gamma_{ext} \simeq 10^{-10} N\ m/\sqrt{Hz}$. The real and imaginary part of $1/\chi_{\theta\Gamma_{ext}}$ are plotted as a function of frequency in fig.29(a) and fig.29(b) respectively. We see that in agreement with eq.15 the real part of $1/\chi_{\theta\Gamma_{ext}}$ is very well fitted by a parabola whereas the imaginary part is linear for small f. The deviation of the data from the linear behaviour is due to the non-newtonian character of the silicon oil at higher frequencies. Once the response is known one can set the external torque to zero and measure S_θ, the spectrum of the thermal fluctuations of θ. In this case the fluctuation dissipation relation is :

$$S_\theta = \frac{4k_B T}{\omega} Im(\chi_{\theta\Gamma_{ext}}) \tag{16}$$

By inserting the measured $\chi_{\theta\Gamma_{ext}}$ in eq.16, we get an estimation of the fluctuation spectrum S_θ. The comparison between this computed S_θ and the measured one is done in fig.30. Except for the existence of the peaks due to environmental noise the agreement is quite good. Thus the rheometer has enough sensitivity to verify FDR in viscous fluids.

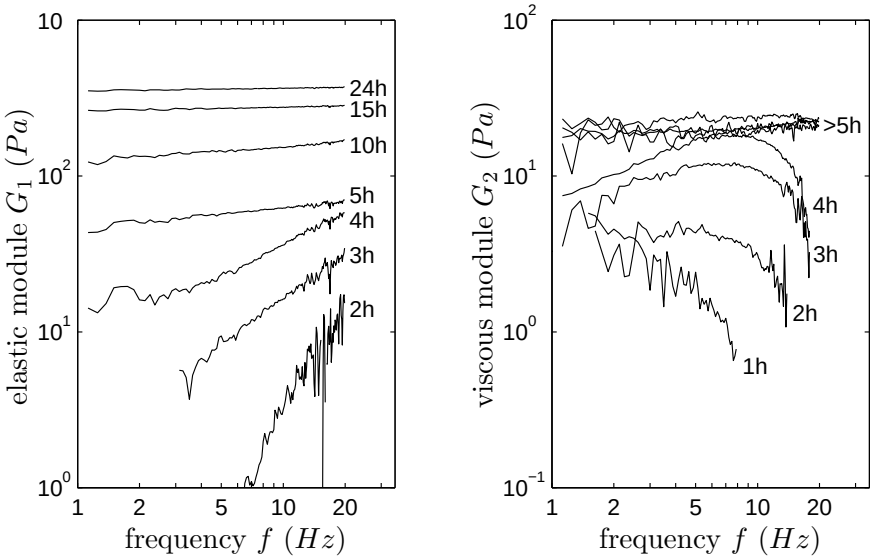

Figure 31: **Aging of the viscoelastic module of Laponite** at a 3% mass concentration in water. The real (a) and imaginary (b) part of the viscoelastic module are plotted as a function of frequency.

3.5.2 FDR on the rheology of Laponite

We have studied the rheological properties of Laponite at 3% mass concentration in water. Laponite has been prepared in the way described in section 2) for electrical measurements and the rheometer is mounted inside a container filled with a clean Nitrogen atmosphere. Moreover, a thin oil layer on top of the Laponite solution ensures no evaporation can occur. We first measure the response at different times t_w after the preparation. The measured elastic and viscous modules of Laponite are plotted as a function of frequency in fig.31 (a)

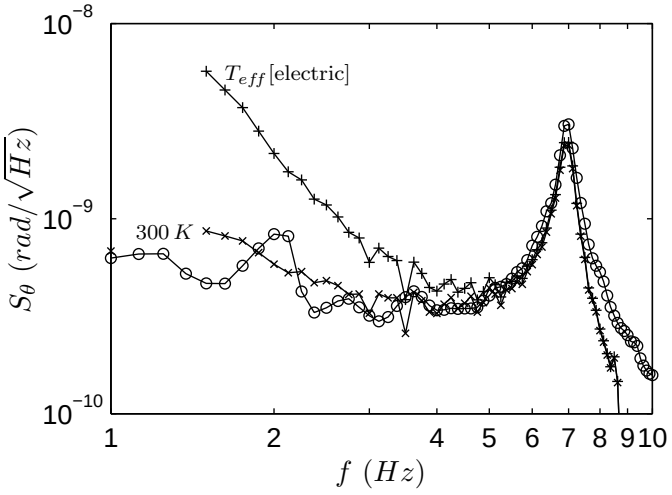

Figure 32: **Thermal fluctuation spectrum of the rheometer filled with Laponite**. The line with $\circ$ is the the result of the measurement. The line with x is the FDT prediction for $T = 300K$. The line with + is obtained from eq.16 by inserting in T the values of T_{eff} estimated from electric measurements.

and (b) respectively. We clearly see that at short t_w the liquid like solution has only viscous response. As time goes on an elastic modulus appears and the viscosity grows of about one order of magnitude. After 24 hours the solution has a solid like aspect with a viscoelastic response. The measurement the thermal fluctuation spectrum S_θ averaged on the first hour of the aging processes of Laponite is plotted in fig.32. The peak at $1.5Hz$ has no physical meaning and is due to a mechanical resonance of the table. Whereas the resonance at $7Hz$ is the resonant frequency of the torsion pendulum of the rheometer. The measure is compared to the prediction of the fluctuation dissipation theorem by inserting in eq.16 the measured values of the Laponite viscous response and $T = 300K$. We also inserted in eq.16 the effective temperature obtained by the electrical measurements averaged on the first hour. We clearly see that in the case of rheological measurements no violation of FDR can be detected within experimental errors. If a violation exists, it is much smaller than that observed in the electric measurements.

3.6 Discussion and conclusions on the effective temperature

Let us resume the main results of the experiments described in the previous sections. We have seen that dielectric measurements of Laponite, during the sol-gel transition, and of polycarbonate, after a temperature quench, show a strong violation of FDT. In agreement with theoretical prediction the amplitude and the persistence time of the FDT violation is a decreasing function of frequency and time. The effective temperature defined by eq.2 is huge at small f and t_w and slowly relaxes towards the bath temperature. In contrast to theoretical predictions the violation is observed even at $\omega t_w >> 1$ and it may last for more than $3h$ for

$f > 1Hz$. We have than investigated the behaviour of the noise signals and we have shown that the huge T_{eff} is produced by very large intermittent bursts which are at the origin of the low frequency power law decay of noise spectra. Furthermore we have also shown that for both materials the statistic of this event is strongly non Gaussian when FDT is violated and slowly relaxes to a Gaussian one at very long t_w. Thus these two very different materials have a very similar relaxation dynamics, characterized by a strong intermittency. This strongly intermittent dynamics is reminiscent of the intermittence observed in the local measurements of polymer dielectric properties [59]. Furthermore recent measurements done, using Time Resolved Correlation in Diffusing wave spectroscopy, have shown a strong intermittency in the slow relaxation dynamics of a colloidal gel [60].

The first striking result which merits to be discussed is the huge T_{eff} measured in Laponite and polycarbonate. Such a large T_{eff} is not specific to our systems but it has been observed in domain growth models [10, 38] and in models controlled by activation processes [42, 43]. The question is whether these models may have some connections with our observations. We have seen that in our experiments the high effective temperature is produced by a very intermittent dynamics. This kind of behavior can, indeed, be interpreted on the basis of the trap model [6, 42], which predicts non trivial violation of FDT associated to an intermittent dynamics. The system evolves in deeper and deeper valleys on the energy landscape. The dynamics is fundamentally intermittent because either nothing moves or there is a jump between two traps. In our case these jumps could explain the presence in the dielectric voltage noise of very large and rare peaks with a slow relaxation after the jump. Clear answers to this question can be given by a detailed study of the statistics of the time intervals between large peaks. This study is in progress.

However it is important to point out that intermittent dynamics and very large T_{eff} are not observed in all the systems. Indeed spin-glass experiments [47, 48] have a behaviour, which, at least for temperatures close to T_g, is coherent to mean field predictions. Instead on the basis of the available experimental data nothing can be said about the supercooled liquid dynamics, because, as we have seen in sec.3.2, only single frequency measurements have been done on these materials.

Another important point that we have discussed is the dependence of T_{eff} on the observable. In sect.(3.3) we have studied this problem by measuring FDR of the rheological properties of Laponite. These measurements show that, within experimental errors, either there is no violation of FDT or this violation is certainly much smaller than that observed in the dielectric measurements. The reasons of this difference between electrical and mechanical measurements are unclear and much work is necessary to give new insight on these problems. However it is important to stress that this difference is coherent with trap models, which predict not only an intermittent dynamics, but also an observable dependent T_{eff}.

4 General conclusions

The purpose of this lecture was that of discussing several experimental approaches which are useful to characterize the aging dynamics. In the first part we have discussed methods based on the analysis of the response functions, showing the existence of very spectacular effects such as memory and rejuvenation. However we have seen that, although these two effects

are extremely useful to fix constraints for the models of aging, the informations extracted by these techniques are not enough to make a distinction among the different models. For this reason in the second part of the lecture we have discussed the measurement of the FDR for different materials and observables. As the FDR is strongly model dependent, the association of thermal noise and response measurements is extremely useful to give new insight on the aging dynamics.

As we have already mentioned many questions are still open. For example it will be very useful to clarify whether the intermittent dynamics is always associated with an observable dependent T_{eff}. Further, it will be important to understand whether the intermittency observed on global variables is related to local rearrangement inside the sample. Much work is needed in order to answer to these questions.

Acknowledgments

We acknowledge useful discussion with J. L. Barrat, L. Berthier, J.P. Bouchaud and J. Kurchan. We also thank E. Vincent for having send us fig.12 and for useful comments on the manuscript.

References

[1] L.C. Struik, *Physical aging in amorphous polymers and other materials* (Elsevier, Amsterdam, 1978).

[2] *Spin Glasses and Random Fields*, edited by A. P. Young, Series on Directions in Condensed Matter Physics Vol.12 (World Scientific, Singapore 1998).

[3] M.Kroon, G. H. Wegdam, R. Sprik, *Dynamic light scattering studies on the sol-gel transition of a suspension of anisotropic colloidal particles*, Phys. Rev. E, 54 , 1 (1996).

[4] K. Jonason, E. Vincent, J. Hammann, J. P. Bouchaud, P. Nordblad, *Memory and chaos effects in spin glasses*, Phys. Rev. Lett. 81, 3243 (1998).

[5] L. Bellon, S. Ciliberto, C. Laroche, *Advanced Memory effects in the aging of a polymer glass*, Eur. Phys. J. B., 25, 223, 2002.

[6] J.P. Bouchaud, D. S. Dean, *Aging on Parisi's tree*, J. Phys. I France, 5, 265 (1995).

[7] D. S. Fisher, D. A Huse, *Ordered phase of short range ising spin-glasses*, Phys. Rev. Lett., 56, 1601 (1986); D. S. Fisher, D. A Huse, *Nonequilibrium dynamics in spin glasses*, Phys. Rev. B, 38, 373, (1988).

[8] E. Bertin, J. P. Bouchaud, *Dynamical ultrametricity in the critical trap model* J. Phys. A-Math. Gen. 35 (13), 3039(2002). Also in cond-mat/0112187

[9] J.P. Bouchaud, L. F. Cugliandolo, J. Kurchan, M. Mézard, *Out of equilibrium dynamics in Spin Glasses and other glassy systems*, in *Spin Glasses and Random Fields*, ed A.P. Young (World Scientific, Singapore 1998). Also in cond-mat/9702070.

[10] L. Cugliandolo, J. Kurchan, L. Peliti, *Energy flow, partial equilibration and effective temperatures in systems with slow dynamics*, Phys. Rev. E 55, 3898 (1997).

[11] L. Cugliandolo, These proceedings.

[12] N. G. McCrum, B. E. Read, G. Williams, *Anelastic and Dielectric Effects in Polymeric Solids*,(Dover 1991)

[13] M. Lederman, R. Orbach, J.M. Hammann, M. Ocio, E. Vincent, *Dynamics in spin-glasses*, Phys. Rev. B, 44, 7403 (1991); E. Vincent, J. P. Bouchaud, J. Hammann, F. Lefloch, *Contrasting effect of field and temperature variations on aging of spin-glasses*, Phil. Mag. B, 71, 489 (1995).

[14] F. Alberici, P. Doussineau, A. Levelut, *New results about aging in an orientational glass*, Europhysics Lett., 39, 329 (1997).

[15] R. L. Leheny, S. R. Nagel, *Frequency-domain study of physical aging in a simple liquid*, Phys. Rev.B 57, 5154 (1998).

[16] T. Jonsson, K. Jonason, P. Nordblad, *Relaxation of the field-cooled magnetization of an Ising spin glass*, Phys. Rev. B 59, 9402 (1999).

[17] P. Doussineau, T. Lacerda-Aroso, A. Levelut, *Aging and memory effects in a disordered crystal*, Europhys. Lett., 46, 401 (1999).

[18] E. Muzeau, G. Vigier, R. Vassoille and J. Perez, *Changes of thermodynamic and dynamic mechanical properties of poly(methyl methacrylate) due to structural relaxation: low-temperature ageing and modelling*, Polymer, 36, (1995), 611.

[19] L. Bellon, S. Ciliberto, C. Laroche, *Temperature cycling during the aging o a polymer glass*. Also in cond-mat/9905160.

[20] L. Bellon, C. Laroche, S. Ciliberto, *Memory in the aging of a polymer glass*,Europhys. Lett., 51, 551 (2000)

[21] K. Jonason, P. Nordblad, E. Vincent, J. Hammann and J.-P. Bouchaud, *Memory interference effects in spin glasses*, Eur. Phys. J. B. 13, 99 (2000)

[22] V. Dupuis, E. Vincent, J.P. Bouchaud, J. Hammann, A. Ito, H. Aruga Katori, *Aging, rejuvenation and memory effects in Ising and Heisenberg spin glasses*, Phys. Rev B 64 (17),174204,(2001). Also in cond-mat/0104399

[23] V. Dupuis, *Dynamique Lente des Systèmes magnétiques Désordonnés*, PhD Thesis, Université de Paris XI, Orsay (2002).

[24] J.P. Bouchaud, V. Dupuis, J. Hamman, E. Vincent, *Separation of time and length scales in spin glasses: Temperature as a microscope*, Phys. Rev. B 65, 024439 (2002).

[25] J. P. Bouchaud, *Aging in glassy systems: new experiments, simple models and open questions, in 'Soft and Fragile Matter: Nonequilibrium Dynamics*, Metastability and Flow', M. E. Cates and M. R. Evans, Eds., IOP Publishing (Bristol and Philadelphia, 2000), 285-304. Also in cond-mat/9910387

[26] A. Kovacs, *La contraction isotherme des polymeres amorphes*, J. Polym. Sci. 30 (1958) 131.

[27] A. J. Bray, M. A. Moore, *Chaotic Nature of the Spin-Glass phase*, Phys. Rev. Lett. 58, 57, (1987).

[28] L. Berthier, P. C. Holdsworth, *Surfing on a critical line: Rejuvenation without chaos, memory without a hierarchical phase space*, Europhys. Lett. 58 (1), 35(2002). Also in cond-mat/0109169v1

[29] E. Vincent, J. Hammann, M. Ocio, J. P. Bouchaud, L. F. Cugliandolo, in *"Complex Behavior of Glassy systems"*, Springer Verlag Lecture Notes in Physics, Vol. 492, M. Rubi Editor, 184, (1997). Also in cond-mat/9607224.

[30] L. Cugliandolo, J. Kurchan, *Analytical solution of the Off Equilibrium Dynamics of a Long Range Spin Glass Model*, Phys. Rev. Lett., 71, 173 (1993).

[31] S.R. de Groot, P. Mazur, *Non equilibrium thermodynamics*, (Dover, 1984)

[32] J.H. Wendorff, E. W. Fischer, *Thermal density fluctuations in amorphous polymers as revealed by small angle X-ray diffraction*, Kolloid-Z. u. Z. Polymere 251, 876 (1973).

[33] H. Sompolinsky, *Time Dependent Order Parameter in Spin Glasses*, Phys. Rev. Lett. 47 935 (1981).

[34] P. Hoenberg, B. Shraiman, *Chaotic behaviour of an extended system*, Physica D, 37, 109 (1989).

[35] G. Parisi, *Off-Equilibrium Fluctuation-Dissipation Relation in Fragile Glasses* Phys. Rev. Lett., 79, 3660 (1997).

[36] W. Kob, J. L. Barrat, *Aging effects in a Lennard Jones Glass*, Phys. Rev. Lett., 78, 4581 (1997);

[37] J. L. Barrat, W. Kob, *Fluctuation dissipation ratio in an aging Lennard-Jones* Europhys. Lett., 46, 637 (1999).

[38] A. Barrat, *Monte-Carlo simulations of the violation of the fluctuation-dissipation theorem in domain growth processes*, Phys. Rev., E57, 3629 (1998).

[39] M. Sellitto, *Fluctuation dissipation ratio in lattice-gas models with kinetic constraints*, European Physical Journal, B4, 135 (1998).

[40] E. Marinari, G. Parisi, F. Ricci-Tersenghi, J. J. Ruiz-Lorenzo, *Violation of the Fluctuation Dissipation Theorem in Finite Dimensional Spin Glasses*, J. Phys. A: Math. Gen., 31, 2611 (1998)

[41] L. Berthier, J. L. Barrat, J. Kurchan, *Two-times scales, two temperature scenario for nonlinear rheology*, Phys. Rev. E, 61, 5464 (2000).

[42] S. Fielding, P. Sollich, *Observable dependence of Fluctuation dissipation relation and effective temperature*, Phys. ReV Lett., 88, 50603-1, (2002).

[43] A. Perez-Madrid, D. Reguera, J.M. Rubi, *Origin of the Violation of the Fluctuation-Dissipation Theorem in Systems with Activated Dynamics*. Also in cond-mat/0210089.

[44] T. S. Grigera, N. Israeloff, *Observation of Fluctuation-Dissipation-Theorem Violations in a Structural Glass*, Phys. Rev. Lett., 83, 5038 (1999).

[45] L. Bellon, S. Ciliberto, C. Laroche, *Violation of fluctuation dissipation relation during the formation of a colloidal glass*, Europhys. Lett., 53, 511 (2001).

[46] L.Bellon, S. Ciliberto, *Experimental study of fluctuation dissipation relation during the aging process*, Physica D, 168, 325 (2002).

[47] D. Herrisson, M. Ocio, *Fluctuation-dissipation ratio of a spin glass in the aging regime*, Phys. Rev. Lett., 88, 257702 (2002). Also in cond-mat/0112378.

[48] M. Ocio, These proceedings

[49] L. Buisson, A. Garcimartin, S. Ciliberto, submitted.

[50] Laponite RD is a registered trademark of Laporte Absorbents, P.O Box 2, Cheshire, UK.

[51] D. Bonn, H. Tanaka, G. Wegdam, H. Kellay, J. Meunier, *Aging of a colloidal "Wigner" glass*, Europhysics Letters, 45, 52 (1999); D. Bonn, H. Kellay, H. Tanaka, G. Wegdam, J. Meunier, Langmuir, 15, 7534 (1999).

[52] R. Hunter, *The foundation of colloid science*, (Oxford Science Publications, 1989)

[53] J.Koryta, L. Dvorak and L. Kavan, *Principles of Electrochemistry* - 2nd Ed. (Wiley, 1993).

[54] C.G. Robertson, G. L. Wilkes, *Long term volume relaxation of bisphenol A polycarbonate and atactic polystyrene*, Macromolecules 33, 3954 (2000).

[55] L. Saviot, E. Duval, J.F. Jal, A.J. Dianoux, *Very fast relaxation in polycarbonate glass* Eur. Phys. J. B., 17 (4), 661, (2000).

[56] R. Quinson, *Caractérisation et modélisation de la déformation non élastique des polymères amorphes à l'état solide,PhD Thesis, (INSA), (1998).*

[57] L. Berthier, J. P. Bouchaud,*Geometrical Aspects of Aging and Rejuvenation in the Ising Spin Glass: A Numerical Study*, Physical Review B. Also in cond-mat/0202069v1

[58] L. Cipelletti, S. Manley, R. C. Ball, D. A. Weitz, *Universal aging features in the restructuring of fractal colloidal gels*, Phys. Rev. Lett., 84, 2275 (2000).

[59] E. Vidal Russel, N. E. Israeloff, *Direct observation of molecular cooperativity near the glass transition*, Nature, 408,695 (2000).

[60] L. Cipelletti, H. Bissig, V. Trappe, P. Ballestat, S. Mazoyer, submitted J. Phys: Cond. Mat.

[61] *Light Scattering by Liquid Surfaces and Complementary Techniques*, ed. D. Langevin (Dekker, New York 1992)

[62] L. Bellon, *Viellissement des systèmes vitreux et rapport fluctution-dissipation*, PhD Thesis, ENS de Lyon,(2001)

[63] L.Bellon, L. Buisson, S. Ciliberto, F. Vittoz, *Zero Applied Stress Rheometer*, Rev. Sci. Instrum., 73 (9), 3286,(2002).

[64] G. Nomarski, *Microinterféromètre différentiel à ondes polarisées*, Journal de Physique. Radium 16, 110 (1955)